Thermal Management of Tungsten by Spectrally Selective Thin Film Optical Filter under Laser Illumination

by
Saina Farrokhpour Sani

Submitted to the Graduate School of f Engineering
and Natural Sciences in partial fulfillment of
the requirements for the degree of Master of Science

Sabancı University
July 2023

ABSTRACT

Thermal Management of Tungsten by Spectrally Selective Thin Film Optical Filter under Laser Illumination

Saina Farrokhpour Sani

Mechatronic Engineering M.S. THESIS, JULY 2023

Thesis Supervisor: Prof. İbrahim Kürşat Şendur

Keywords: Radiation, Thermal management, Optics, Spectrally selective optical filters, Distributed Bragg reflectors

Surface temperature management of refractory metals, such as Tungsten, is crucial for their use in high-temperature applications like aerospace, defense, and laser instruments. In the presented work, distributed Bragg reflectors (DBR) are utilized to reduce the temperature caused by intense laser illumination. To address this problem, we developed a coupled optical and thermal model and investigated multiple factors, including material composition, morphology, architecture, and source-related parameters, such as wavelength. Our results indicate that our DBR coating designs can significantly decrease the temperature of the Tungsten. Moreover, we observed that at higher laser power, the radiative heat transfer and surface emissivity play a prominent role in decreasing temperature, contributing to 32% of the cooling processes. However, at low laser powers, conductive heat transfer is the dominant mechanism, which accounts for 93%.

ÖZET

Lazer Aydınlatması Altında Spektral Olarak Seçici İnce Film Optik Filtreler ile Tungsten'in Termal Yönetimi

Saina Farrokhpour Sani

MEKATRONIK MÜHENDISLIĞI YÜKSEK LİSANS TEZİ, TEMMUZ 2023

Tez Danışmanı: Prof. Dr. İbrahim Kürşat Şendur

Anahtar Kelimeler: Radyasyon, Termal yönetim, Optik, Spektral olarak seçici optik filtreler, Dağıtılmış Bragg yansıtıcılar:

Tungsten gibi refrakter metallerin yüzey sıcaklığı yönetimi, havacılık, savunma ve lazer cihazları gibi yüksek sıcaklık uygulamalarında kullanımları için çok önemlidir. Sunulan çalışmada, yoğun lazer aydınlatmasının neden olduğu sıcaklığı azaltmak için dağıtılmış Bragg yansıtıcılar (DBR) kullanılmaktadır. Bu sorunu ele almak için, birleşik bir optik ve termal model geliştirdik ve malzeme bileşimi, morfoloji, mimari ve dalga boyu gibi kaynakla ilgili parametreler dahil olmak üzere birçok faktörü araştırdık. Sonuçlarımız, DBR kaplama tasarımlarımızın Tungsten sıcaklığını önemli ölçüde azaltabileceğini göstermektedir. Ayrıca, daha yüksek lazer gücünde, radyatif ısı transferi ve yüzey emisyonunun, soğutma işlemlerinin %32'sine katkıda bulunarak sıcaklığın düşürülmesinde önemli bir rol oynadığını gözlemledik. Bununla birlikte, düşük lazer güçlerinde, iletken ısı transferi baskın mekanizmadır ve %93'ünü oluşturur.

ACKNOWLEDGEMENTS

"No one who achieves success does so without acknowledging the help of others. The wise and confident acknowledge this help with gratitude". To this end, I would like to express my deepest gratitude to whom believed in me more than I believed in myself, my thesis advisor for all the lessons I have learned from him, and for his invaluable patience, professional and emotional support, and feedback.

I would thank The Scientific and Technological Research Council of Turkey (TÜBİTAK) for supporting this project. The project number is 120F152.

Finally, I would be remiss in not mentioning my family, my love Mosayeb, and my friends. My spirit and motivation have remained strong because of their belief in me during this process.

Dedicated

To my beloved family and

the martyrs on the way to the freedom of my homeland.

TABLE OF CONTENTS

LIST OF TABLES ..... **ix**

LIST OF FIGURES ..... **x**

1. INTRODUCTION..... **1**

1.1. Literature Survey 3
1.1.1 Distributed Bragg reflectors 3
1.1.2 Thermal management using thin films reflectors..... 4
1.1.3 Patterning of Distributed Bragg reflectors..... 5

1.2 Objectives 6

1.3 Contributions 7

1.4 Thesis Outline..... 9

2. AN OPTICAL STUDY ON ENHANCING REFLECTANCE OF REFRACTORY METALS BY SPECTRALLY SELECTIVE THIN-FILMS FILTER DESIGN **10**

2.1. Methodology..... 10
2.1.1. Distributed Bragg Reflectors 11
2.1.2 Thickness calculation 15
2.1.3 Reflectance calculation for a DBR..... 16
2.1.4 Materials for DBRs..... 19

2.2. Model and simulation..... 21

2.3. Results and discussion..... 28 29

3. A THERMAL STUDY ON DECREASING THE TEMPERATURE IN REFRACTORY METALS SUBJECTED TO AN ELECTROMAGNETIC WAVE BY SPECTRALLY SELECTIVE THIN-FILMS FILTER **38**

3.1. Methodology……...… …… 39

3.2. Model and simulation……..… …… 40

3.3. Results and discussion……..… …… 42 29

4. AN OPTICAL STUDY ON ENHANCING REFLECTANCE OF REFRACTORY METALS BY PATTERNING **50**

4.1. Cavity enhanced DBR……...… …….. 51

4.2. Patterned cavity enhanced DBR……...… …… 55

5. CONCLUSION…… **60**

BIBLIOGRAPHY…… **63**

LIST OF TABLES

Table 2.1. results of thickness calculation for different wavelengths in a DBR composed of TiO_2 and SiO_2 layers (Thicknesses are in nm)……..……...… 15

Table 2.2. some material properties of thin films……..…...…….. 21

Table 2.3. available commercial laser devices operating at wavelengths near 700 nm…...… 26

Table 2.4. Optimized thicknesses for different materials based on Equation 2.7…… 31

Table 2.5. Effect of thickness optimization on the average Reflectance …….31

Table 2.6. Effect of the number of layers on the average Reflectance…… 34

Table 2.7. Effect of the number of layers on the emittance at 700nm.....35

Table 3.1. the emissivity of different materials in a 10-layer DBR obtained from the absorptance curves……... 42

Table 3.2. Important material properties used in heat transfer modeling in COMSOL……...42

LIST OF FIGURES

Figure 2.1. The incident, reflected, and absorbed light for (a) uncoated refractory metal and (b) coated by DBR refractory metal……11

Figure 2.2. the angles of incident and refracted waves in three different mediums……..12

Figure 2.3. Reflected beams in a DBR ……14

Figure 2.4. plane wave incident on a thin film……..16

Figure 2.5. Schematic of a multilayer structure exposed to a Gaussian laser beam at different locations along the propagation axis ……..25

Figure 2.6. The effect of the divergence angle of the laser beam on the maximum temperature…….. 27

Figure 2.7. the schematic of the COMSOL model for coated and uncoated substrate…..27

Figure 2.8. Reflectance, absorptance, and transmittance of uncoated Tungsten……...28

Figure 2.9. The effect of adding 6 layers of coating on top of the Tungsten substrate on Reflectance ……30

Figure 2.10. The effect of thickness optimization on Reflectance of SiO_2, TiO_2 multilayers…….32

Figure 2.11. The comparison of the Finite Element and Transfer Matrix methods……..32

Figure 2.12. The comparison of the effect of the number of layers on Reflectance…….33

Figure 2.13. The comparison of the effect of the material choice on reflectance…….36

Figure 2.14. The comparison of the effect of the angle of incidence on the reflectance...36

Figure 3.1. A schematic of temperature distribution in a refractory metal and a DBR structure on top of that and the heat transfer mechanisms participating in the energy balance of the structure…….38

Figure 3.2. A schematic of the thermal loads and boundary conditions of the design…..41

Figure3.3. temperature variation during the time for the input power of (a) 1.443×10-6 (b) 1×10-8 (c) 1×10-9 ……. 45

Figure 3.4. Temperature variation during the time for different material choices and a) Low-power, b) Medium-power, and c) High-power case...……..47

Figure 3.5. The comparison of the effect of the angle of incidence on the Temperature..48

Figure 3.6. Temperature changes versus the number of layers for different pairs of materials..…….. 49

Figure 4.1. Multiple light beam reflections inside a cavity between two stacks of DBR..51

Figure 4.2. A schematic of a cavity enhanced DBR on top of the Tungsten substrate…..52

Figure 4.3. Reflectance comparison for different thicknesses of the cavity layer…….53

Figure 4.4. Electric field comparison for different thicknesses of the cavity layer…….54

Figure 4.5. Allowed longitudinal resonant mode inside a cavity. ……55

Figure 4.6. The periodic configuration of patterned cavity enhanced DBR configuration. A) An oblique view, and b) 2D view.. ……56

Figure 4.7. Schematic of a unit cell of a cavity enhanced patterned DBR on top of the Tungsten substrate. a) Oblique view, and b) 2D view showing the cavity layer with the thickness of L……57

Figure 4.8. Reflectance comparison for different thicknesses of the cavity layer in patterned DBR structure. ……..58

Figure 4.9. Electric field comparison for different thicknesses of the cavity layer a)300nm, b)500nm, c)700nm, and d)900nm. ……58

1. INTRODUCTION

Tungsten has attracted interest recently due to its remarkable thermomechanical properties. Due to its superior melting properties, tungsten is frequently used in high-temperature products like electrical contacts, furnace parts, and welding electrodes[1, 2]. Tungsten has the highest melting point of any metal. Tungsten is a valuable material for creating cutting tools like drill bits and saw blades since it is also strong and durable[2, 3] and improves the strength of alloys[4-6]. Due to its excellent electrical conductivity, tungsten is utilized to make the filaments for electronic equipment like vacuum tubes and incandescent light bulbs[7]. In the medical sector, tungsten is also employed as radiation-shielding material to shield patients and medical professionals during diagnostic and therapeutic treatments. Several industrial uses, including those in the chemical, aerospace, and auto industries, require tungsten[8]. These attractive thermomechanical properties make it a good candidate for spacecraft applications, welding, and other high-temperature applications[9-11]. Despite the aforementioned attractive features, tungsten's high absorptance can create heating problems, particularly when the surface is exposed to high levels of radiative infrared thermal load.

Here, our aim is to reduce the transferred heat to the Tungsten substrate from the light beam by means of increasing the surface’s reflection. When a laser beam is incident upon a surface, it can be reflected, absorbed, or transmitted. The amount of reflection depends on the surface's reflectivity[12]. Therefore, the reflectivity of the target is an important consideration. Highly reflective surfaces, such as mirrors or polished metals, can reflect the laser beam away from the target and reduce the amount of energy delivered to the intended target. Therefore, surfaces with low reflectivity such as rougher[13] matte surfaces will absorb more energy from the laser beams.

Tungsten is a good reflector for incident thermal radiation when the incident wavelength is larger than 1500 nm. However, Tungsten has relatively poor reflectivity over the visible and near-infrared spectral regions[14]. As a result, one of the main challenges of its use in high infrared radiation applications is that it absorbs a significant portion of the incident

thermal radiation for wavelengths below 1500 nm. In the literature, it was reported that the absorption percentages of refractory metals in the 300–1500 nm spectrum vary from 40% to 50%. To overcome this problem several multilayer structures have been designed to enhance the surface reflectivity[14]. High-quality mirrors for scientific and industrial uses, including telescopes and laser systems, are also made with tungsten. Tungsten mirrors can keep their form and reflectivity across a wide temperature range because they have a high reflectivity and a low coefficient of thermal expansion[8].

High reflective structures also have applications in laser lightening such as color conversion materials to achieve white light such as quantum dots[15], high-performance light-emitting diodes, and applications in display and lighting industries[16], converters for high-power solid-state light sources[17], QLEDs as energy-efficient alternatives to traditional lighting technologies such as incandescent bulbs and fluorescent lamp[15-19].

Tungsten has one of the lowest coefficient of thermal expansion of any pure metals and the highest melting point of all refractory metals. Tungsten is largely used in rocket propulsion systems and solar thermal thrusters[20], antimatter propulsion[21], high-temperature aircraft and rocket engine turbine[18], micro thruster[22], and passive space radiation shielding[23]. In all these applications, the environment in aircraft or spacecraft presents a severe set of operating conditions such as high temperatures. Therefore, it is crucial to improve the thermal characteristics of tungsten.

Generally, refractory metals such as Tungsten have relatively low reflectance. For Tungsten reflectance is about 0.4 in 300-1000 nm wavelengths. This spectrum includes visible and infrared light and many laser beams operated in this range. So, if they are exposed to a laser beam, most of the energy is absorbed, and as a result, the temperature increases inside the metal. To overcome this problem, using reflectors and mirrors on top of the metal substrate is a potential solution.

1.1 Literature Survey

In this section, the relevant literature review for the topics discussed in this study is presented. The objective of this section is to realize the missing aspects in the relevant literature, primarily. Afterwards, the potential solutions, which are the main aim of this dissertation, will be discussed.

1.1.1 Distributed Bragg reflectors

Distributed Bragg reflectors (DBRs) are well-known for increasing the reflectivity of a surface, especially used for optical communications[24]. The concept of DBRs can also be used to decrease the radiative thermal load in the thermal infrared regions by coating the material surface with periodic high-index and low-index layers. While the concept of DBRs was used to increase the reflectivity in the literature for optical communications[25] an important consideration for radiative thermal load in the infrared is not only the amplitude of reflectivity but also the bandwidth of operation. These concerns can be addressed by the material composition[26], the number of layers[27], roughness[28-32], and thickness of the layers[33-36]. The reflectivity of DBRs is high in a specific range of wavelengths, which is defined as a stopband[37]. It has been shown that as the number of the layers in a DBR increases the reflectance of the structure increases too[38, 39]. Also, thickness of the layers should be chosen carefully based on quarter-wavelength rule using Transfer Matrix Method. The thickness is dependent to the material's refractive index, angle of incident, and the targeted wavelength of the filter[40, 41]. Other researches showed that decreasing the surface roughness is an important factor in increasing the reflection[42]. By controlling all factors, we can design a DBR to use as a coating for the Tungsten substrate to increase the reflection from the surface and decrease the maximum temperature.

In the literature, various heat mirror multilayers based on tungsten substrate or tungsten oxide multilayers have been fabricated[43-46]. A study on tungsten oxide and silver showed that the visible transmittance decreased as the thickness of the silver layer increased, and

therefore, the infrared reflectance increased as the thickness of the silver layer increased[44]. In other words, increasing the thickness of the substrate decreases the transmittance, so the reflectance increases. However, in the case of Tungsten, it is an opaque metal that absorbs the light that goes inside it. This means that changing the thickness of tungsten is not helpful for increasing the reflectance by decreasing the transmittance. The combination of Anti-reflectors and DBRs is named a cold mirror and is capable of reflecting the visible wavelength band and transmitting the infrared wavelength band[47, 48] or vice versa[49], or even reflecting both bands[50], and temperature curves show a reduction in temperature while using cold mirrors (for example TiO_2, SiO_2 mirrors) compared to the case of the structure without any mirrors[51]. The fabrication of these multilayers has been addressed in the literature[52-57]. However, there is no sufficient research on the influence of designing and attaching a suitable DBR on the tungsten substrate's reflectance, emittance, and the amount of temperature increment under high-power laser illuminations.

1.1.2 Thermal management using thin film reflectors

In recent years, several studies have been conducted to reduce the radiative thermal load in Tungsten by using multi-layer thin films. The effect of spectrally selective reflectors on a solar cell system showed that it reduces heating by reflecting in the 300-1100 nm spectral range[58]. Several designs for passive radiative daytime cooling have also been proposed by utilizing DBRs. For instance, by using TiO_2, SiO_2, and Al_2O_3 layers stacked to refractory metals like Au, W, Mo, and Nb, the reflection of the thermal radiation in visible and near-infrared spectra can be tailored[14, 59]. As a result, in aerospace applications operating in earth orbit, the absorbed irradiance can be reduced[60-62].

In all of the mentioned studies, the aim is to reduce the maximum temperature which is caused by the broadband thermal loads. However, we are interested in controlling the thermal loads in a substate caused by a single wavelength as a high-power laser beam. This means that we need to use dielectric materials as a coating that have a high thermal resistivity and melting point which can perform adequately under harsh thermal loads. There is no sufficient research on the accomplishment of dielectric DBRs in managing the thermal loads caused by a laser beam.

In addition to TiO_2, SiO_2, and Al_2O_3 layers, various reflective coating materials have been reported in the literature. Polymer dielectric mirrors are reported to be able to selectively reflect near-infrared radiation while being highly transparent in the visible range. Simple, tandem, and super periodic mirrors are used to shield radiation[49]. The optical-mechanical and thermal properties of MgF_2-ZnS and MgF_2-Ta_2O_5 composite films were also examined in the literature[63]. Several studies are focused on designing antireflection coatings to enhance the transmissivity of the structure based on TiO_2/SiO_2 and TiO_2/MgF_2 multilayers[64, 65]. Different materials also showed similar results by using anti-reflective coatings on the aluminum substrate[66]. While there are studies exist involving multilayer films to engineer the spectral reflection, transmission, and absorption of surfaces, correlating the infrared radiation load to the temperature distributions over the structures and an investigation of the spatiotemporal thermal characteristic of these processes is largely overlooked in the literature.

In this study, we demonstrate that the radiative thermal infrared load on the Tungsten surfaces can be significantly reduced by using engineered multilayered structures. Moreover, we investigated the effect of these multi-layers on the heat transfer when they are coated over a Tungsten layer. Spatio-temporal characteristics of the thermal processes on the Tungsten layer coated with multilayers have been investigated when the entire surface is subjected to irradiation by a Gaussian laser beam. Also, in this study, we compared different material selections and the effect of geometric parameters on spectral reflection and temperature.

1.1.3 Patterning of Distributed Bragg Reflectors

Distributed Bragg Reflectors (DBRs) have emerged as highly efficient components for precise control of light wavelengths and exceptional reflectivity in various optical applications, including optical filters. However, when operating under high-temperature conditions such as intense laser illuminations, the presence of thermal stresses poses a significant challenge to DBR performance. The effects of temperature on the center wavelengths of DBRs are measured and calculated. The shift of the center wavelength can be about 0.1 nm for every 1K change in temperature[67-70]. These thermal stresses can lead to expansion within the DBR structure, potentially resulting in peeling, deformation, or other forms of damage if there is insufficient space for expansion[71, 72]. Cracking due

to a large mismatch of the thermal expansion between layers of the DBR and the substrate is the common failure mode[73-75]. Also, one of the common problems that has been observed is the fragility of DBR layers, especially when exposed to thermal stresses. In this case, bubbling and cracking has been observed[76, 77]. On top of that, temperature increases may alter the reflection of the design by changing the refractive index of the layers under thermal stresses[78]. Refractive index coefficient of some dielectric films can change up to ten times less by changing the temperature[78, 79]. Same situation is possible to occur for metals such as Tungsten[69].

These challenges can be addressed by patterning the DBR structure. Patterning allows to make some intervals in the structure so the expansion can happen freely and decrease the thermal stresses. For example, while a coated substrate heats up or cools down, the stresses can be induced because of the difference in the thermal expansion coefficient between the layers which is controllable by patterning the layers[80]. In the literature, considerable stress relief has been obtained by patterning the coating into rectangles and stripes[81]. With rectangular patterns the biaxial stress is degraded to a uniaxial stress and shape and size of the pattern is a key factor in stress reduction[82, 83]. Another example is the thermal stresses developed by temperature gradients involved in the deposition processes. Studies showed that pattern has a significant effect on the part stresses and deflections[84]. Understanding and mitigating these thermal stresses are essential to achieve the full potential of DBRs in high-temperature applications.

1.2 Objectives

The main aim of this thesis is the thermal management of refractory metals by broadband engineering of reflection from the surface using thin-film optical filters such as Distributed Bragg Reflectors. Various methods that combine the material properties, structural combination, and geometry of the coatings are used to design the structures. In the very first step, the reflectance of the bare Tungsten will be calculated. Then, employing commercial software, we will study the reflection of the Tungsten covered by a DBR coating. The efficiency of the coating will be enhanced by optimizing different factors such as material choice, number, and thickness of layers at the targeted wavelength. The incident angle of

the beam light is another crucial factor to be studied. The verification of the results will be performed by comparing the FEM and FDTD models.

Tungsten's surfaces also can be protected from the radiative thermal load by an engineered multilayer coating. Here, we will study the effect of these multi-layers on the maximum temperature when they are coated over a Tungsten layer. Spatio-temporal characteristics of the thermal processes on the Tungsten layer coated with DBR will be investigated when the entire surface is subjected to irradiation by a Gaussian laser beam. We will study and compare different material selections and the effect of geometric parameters on spectral reflection and maximum temperature of the design. Again, the incident angle of the beam light is another factor crucial to be studied. The temperature will be studied for three different pawer magnitudes. At the end, a comprehensive comparison of the different factors will be conducted to make sure that the optimized design provides the best efficiency among all available options for material choice and number of layers.

Furthermore, the effect of cavity or spacer layer on the reflection of the designed structure will be investigated. The thickness of the cavity layer is a key factor to control the bandwidth and amplitude of the reflection. Due to the thermal stresses that the DBR goes through in high temperatures, patterning if the DBR will be studied as a potential solution to reduce the stresses and protect the design from unwanted damages like deformation or peeling.

1.3 Contributions

Here are contributions of the work to the field briefly mentioned:

- Design of a Multilayer structure (Distributed Bragg Reflector) and develop optical model to decrease the absorbance of Tungsten substrate's surface under laser beam illumination; Different parameters such as material choice, angle of incident, thickness, and number of layers have been optimized to achieve a suitable Distributed Bragg Reflector. The results have been verified by Transfer Matrix Method.

- Study of the thermal loads and temperature changes in the structure as a result of absorption of the laser beam energy; When the laser beam interacts with the structure, a portion of its energy is absorbed, subsequently transforming into heat. This study aims to establish a comprehensive understanding of the relationship between the absorbed light energy and the resultant thermal load experienced by the structure. By analyzing this connection, we can gain insights into the thermal behavior, heat distribution, and temperature changes within the structure as a consequence of laser energy absorption.
- Quantifying the emitted heat from the structure under laser illumination; When the structure was subjected to incident laser beams, the heat generated within the structure transferred through various mechanisms, including conduction, convection, and radiation. However, it is important to note that radiative heat transfer is a nonlinear function of the temperature. As the temperature increment increased, particularly in the case of higher powers of incident laser beams, we anticipated a greater contribution of radiation heat transfer from the structure. This nonlinear relationship highlighted the significance of understanding the interplay between incident laser power, temperature increment, and the resulting radiative heat transfer in order to accurately assess the thermal behavior and heat dissipation characteristics of the structure under laser illumination.
- Studying the effect of adding cavity between DBR and tungsten on the surface reflectance; Various thicknesses of the cavity layer have been examined to determine their effect on reflectance. The objective is to identify the optimal thickness that can induce resonance modes, leading to enhanced reflection from the surface. By systematically studying the relationship between cavity thickness and surface reflectance, valuable insights have been gained into the design and optimization of the structure for improved reflective properties.
- Studying the effect of patterning the DBR on the surface reflectance; Patterning the DBR leads to a reduction in its surface area. This decrease in surface area can result in a decrease in overall efficiency. However, when subjected to high-power laser illumination, thermal stresses are induced, posing a risk of mechanical deformation or failure within the structure. Therefore, it becomes essential to pattern the DBR to alleviate these stresses and ensure structural integrity. In this study, we explored the patterning of the DBR and investigate

the influence of cavity thickness and the patterned DBR on the reflection properties of the structure.

A scientific paper resulting from the research presented in this dissertation is currently under review, in the International Journal of Thermal Science with the title of "Thermal Management of Tungsten by Spectrally Selective Thin Film Optical Filters under Laser Illumination." and additional work is being prepared. Furthermore, a poster titled "Thermal Aspects of Distributed Bragg Reflectors" was presented at the FOTONIK Conference in 2022.

1.4 Thesis Outline

The thesis is composed of 5 chapters, in all of which methods and corresponding results, discussions are given for the specific area and the dissertation ends with final conclusions.

In chapter 2, we will introduce Distributed Bragg Reflectors, and the method to find the characteristic matrix for the thin film and extend this matrix for a DBR. A brief discussion on the material and thickness that are chosen is provided as well. In chapter 3, the objective is to study the thermal merits of using DBRs in reducing the temperature and investigating the behavior of the temperature change during the time. As mentioned before, the main objective of this study is to decrease the maximum temperature of the Tungsten substrate. Combining the electromagnetic studies with the heat transfer investigations is essential to have a general view of the mechanisms that are governing the heat and energy transferred in the multilayer structure. In chapter 4, a novel method for increasing the DBR performance has been introduced. The effect of implementing a cavity layer between the DBR and the refractory metal will be discussed. Also, patterning of the DBR is investigated as a solution to prevent any peeling caused by thermal stresses under high power laser illumination. Chapter 5 is dedicated to the final and most important conclusions and the author’s suggestions for future works.

2. AN OPTICAL STUDY ON ENHANCING REFLECTANCE OF REFRACTORY METALS BY SPECTRALLY SELECTIVE THIN-FILMS FILTER DESIGN

Tungsten is one of the most abundant among the refractory metals. It has a very high melting point (3380˚C) and one of the highest metal densities in comparison to other refractory metals. It can become very hard when it is combined with other elements such as carbon[85]. Therefore it is mostly used in applications like aerospace, laser, illusion, and optical instruments[86]. Refractory metals such as Tungsten have a relatively low reflectance (about 0.4) in 300-1000 nm wavelengths range. So, if they are exposed to a laser beam, most of the energy is absorbed, and as a result, the temperature increases inside the metal. To overcome this problem, one can consider using reflectors and mirrors on top of the metal substrate. In this chapter, first, the effect of Distributed Bragg Reflectors on the reflectance enhancement of a substrate in a specific wavelength range is studied. Then, the objective is to investigate the impact of different factors on the widening and improvement of the efficiency of the mentioned reflector.

2.1 Methodology

In this section, we will introduce Distributed Bragg Reflectors, and the method to find the characteristic matrix for the thin film and extend this matrix for a DBR. As the characteristic matrix is obtained, reflectance of the DBR structure can be defined. A brief discussion on the material and thickness chosen is provided as well.

2.1.1 Distributed Bragg Reflectors

Distributed Bragg Reflectors (DBRs) consist of alternating high and low refractive index material layers (Figure 2.1) and are one of the common mirrors[37]. The reflectivity of DBRs is high in a specific range of wavelengths, which is defined as a stopband[14]. As it is shown in Figure 2.1, incident light is decomposed into two reflected and absorbed components. In an uncoated metal (Figure 2.1.a), the portion of absorbed light is relatively bigger than the one in coated material and the portion is illustrated by the arrows' thickness. On the other hand, in Figure 2.1.b the portion of the reflected beam is greater which shows the effect of adding a DBR on top of the refractory metal for reflection enhancement. The high-index and low-index materials can be chosen from a variety of options[26] which we will discuss in this chapter. To have a better understanding of how DBRs work and increase their reflectivity, first a review of the reflection calculation for a multilayer is essential.

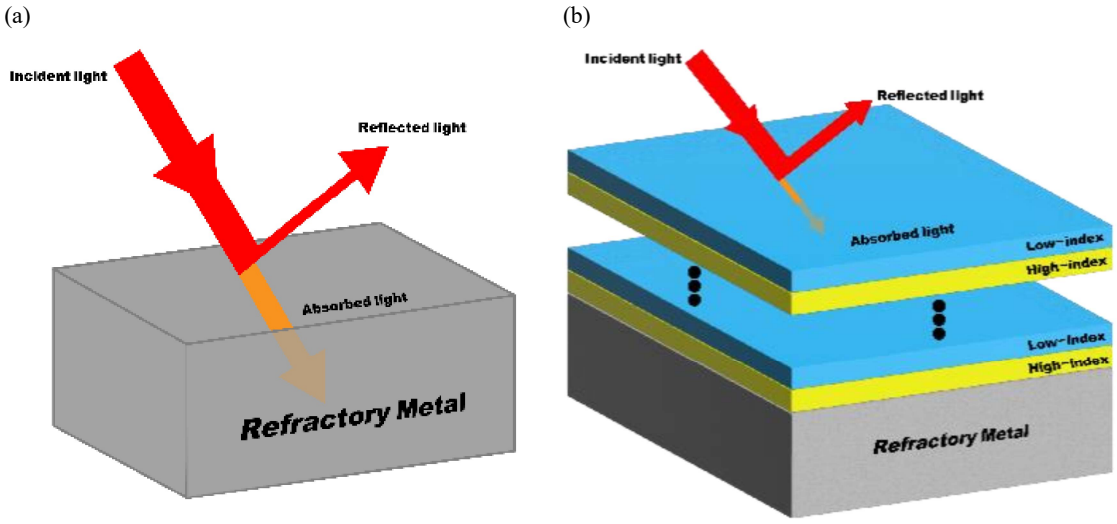

Figure 2.1. The incident, reflected, and absorbed light for (a) uncoated refractory metal and (b) coated by DBR refractory metal.

Reflection is the process in which electromagnetic radiation is reflected at the boundary between two media. Absorption is the transformation of radiated power to another type of energy, usually heat, by interaction with matter. Transmission is the passage of electromagnetic radiation through a medium[87].

In general, a reflecting surface is a boundary between two materials of different electromagnetic properties[87], such as the boundary between air and glass, air and water, or air and metal. Devices designed to reflect radiation are called reflectors or mirrors.

The relationship between the transmitted or reflected ray angle and the incident ray angle follows Snell's law, and the law of reflection concerns the incident and reflected rays and the normal to the reflecting surface in the same plane.[88]:

$$n_1 sin\theta_1 = n_2 sin\theta_2 = n_3 sin\theta_3 \quad (2.1)$$

Where n_1, n_2, and n_3 are the refractive indices for the first, second, and third medium, and θ_1, θ_2 , and θ_3 are the angles of incident and reflected (or transmitted) rays with respect to the normal, respectively (Figure 2.2).

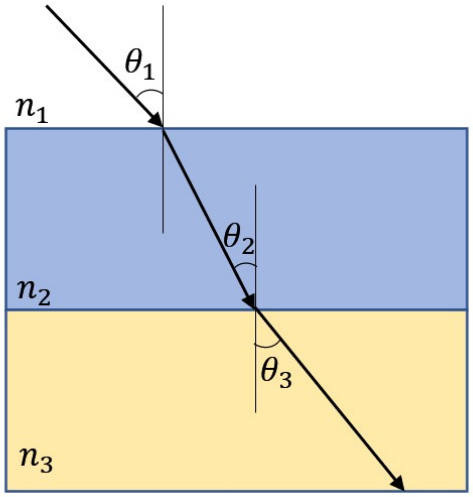

Figure 2.2. the angles of incident and refracted waves in three different mediums

For the case of DBRs, we discuss the normal incident, and all of the formulations are retrieved from[41, 89]. The amplitude reflection coefficient, r, going from material 1 to material 2 is defined as:

$$r = \frac{E_{0r}}{E_{0i}} = \frac{n_2 - n_1}{n_1 + n_2} \quad (2.1)$$

where E_{0r} and E_{0i} are the amplitudes of the reflected and incident electric fields respectively, and n_1 and n_2 are the refractive indices of material 1 and 2 respectively. Reflectance, named R, is defined as the ratio of the reflected power to the incident power:

$$R \equiv \frac{E_{0r}^2}{E_{0i}^2} = r^2 = \left[\frac{n_2 - n_1}{n_1 + n_2}\right]^2 \tag{2.2}$$

As can be seen from the equation above, a greater contrast in the refractive index results in a greater reflectance. Phase transitions at the material contact are also mentioned. If n_2 is greater than n_1, then r will be positive, indicating that the electric fields of the incident and reflected waves are in phase. At the boundary, a -phase shift is required for this to happen. But if n_1 is greater than n_2, then r will be negative, indicating that the reflected wave is out of phase with the incident wave and that there is no phase shift at the interface.[89]. We will discuss the details of the phase change in this chapter. On the other hand, Transmission is:

$$t = \frac{2n_1}{n_1 + n_2} \tag{2.3}$$

From this Equation, we can understand the fact that t will always be positive, so no phase shift occurs for transmitted light. The results for reflection and phase change at interfaces can be exploited to create a mirror with large reflectance.

The absorptance A in a material is connected with transmittance T and reflectance R by the relation:

$$R + T + A = 1 \tag{2.4}$$

Here, we assume that transmittance is zero so we can imply:

$$R + A = 1 \tag{2.5}$$

This means if we increase the reflectance of a structure, absorptance will be decreased; therefore, the absorbed energy will be reduced in the medium.

One should accept two basic concepts [88, 89] to understand the phase of reflected light. First, there is a phase shift of 180˚ when the reflectance takes place in a medium with a lower refractive index than the adjacent medium and of zero if the medium has a higher index than the one that is adjacent. Second, if the light is divided into two elements by reflection at the top and bottom inside surfaces of a thin film, if the relative phase shift is 180˚, then the beams will recombine so that the amplitude of the total reflected beam will be the difference of the amplitudes of the two components. Nevertheless, if the relative phase shift is either zero or 360˚, it is the sum of the amplitudes of two components. In the first case, we say that the beams are destructive, and in the second case, constructive. For different phase shifts, it will be between these

two possibilities. Figure 2.3 illustrates the reflected light as a combination of all reflected lights of each layer.

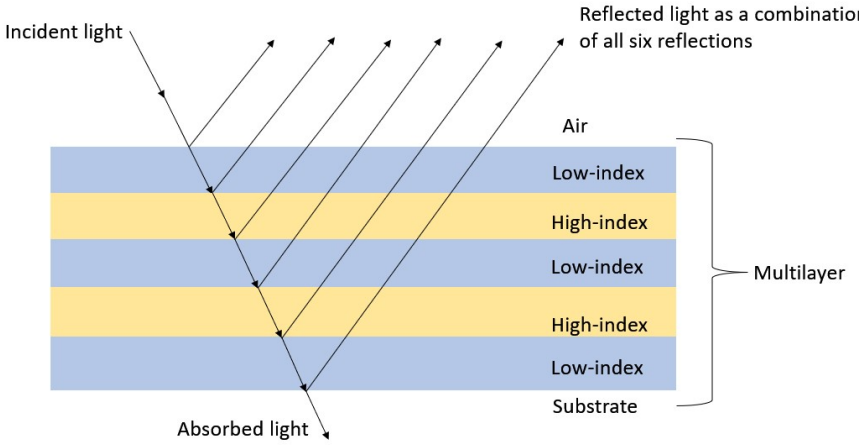

Figure 2.3. Reflected beams in a DBR

In a BDR (Figure 2.3), to achieve constructive interference, layers with thicknesses of a quarter of incident wavelength that is equivalent to a π /2 phase shift, are used. Hence, when the light propagates into a layer and travels in the same layer to come to the surface, it travels a distance of λ/2 per layer which is equivalent to a phase shift of π. The total phase shift will be if the light passes through an odd number of layers before reflection, but if it passes through an even number of layers, there won't be any phase shift because of cancellation. The phase shift caused by the low-to-high index barrier is another thing that has been mentioned previously. If the top layer is made of a high index material, the reflection will be from high to low after passing through an odd number of levels, resulting in no phase shift and an overall -phase shift for an odd number of layers. When going through an even number of layers, the reflection takes place at a low-to-high interface, causing a -phase change. This combination, together with no phase shift, results in a reflection at the surface with a -phase shift. Even if we take into account the effect of many reflections in the layers, the reflected lights are all in phase on the front surface in this case [41].

Therefore, the various components of the incident light produced by reflection at successive boundaries throughout the assembly will reappear at the front surface all in phase so that they will recombine constructively. This is the basic form of high-reflectance coating. When such a coating is constructed, it is found that the reflectance

remains high over only a limited range of wavelengths, depending on the ratio of high and low refractive indices. Outside this zone, the reflectance changes abruptly to a low value.

2.1.2 Thickness calculation

The location of the high reflection zone in DBR can be controlled by adjusting the thicknesses of the periodic layers. By setting the optical thickness of the layers to π/2 at a specified wavelength, high reflection around that wavelength is achieved. The relationship between the optical and geometrical thickness of a layer is given as[11, 41]:

$$\delta_r = \frac{2\pi N_r d_r cos\theta_r}{\lambda} \tag{2.6}$$

where δ is the optical thickness, Nr is the complex refractive index (n-ik), dr is the geometrical thickness, θr is the angle of refraction, and λ is the wavelength. From this Equation, thickness is obtained to find the required film thicknesses to achieve a high reflection zone around the selected wavelength. In Table 2.1, you can find the thickness calculated for different wavelengths Of TiO_2 and SiO_2.

Table 2.1. Results of thickness calculation for different wavelengths in a DBR composed of TiO_2 and SiO_2 layers (Thicknesses are in nm).

Central wavelength	TiO_2 layers thickness	SiO_2 layers thickness
500	41	85
600	51	102
700	62	120
800	71	137
900	81	154

The designs imply that a high precision may be required to control the thickness of the individual thin-film layers that comprise the DBR. However, the deposition of the layers with these thicknesses is feasible. Silicon dioxide (SiO_2) and titanium dioxide (TiO_2) can be deposited utilizing a range of techniques, including Physical Vapor Deposition (PVD) and Chemical Vapor Deposition (CVD). In these methods, the film thickness can be accurately controlled by adjusting the deposition time or the deposition rate. The deposition rate typically falls within the range of 1-100 Å/s, enabling precise control over layer thickness with Angstrom-level precision[90-92].

2.1.3 Reflectance calculation for a DBR

In this section, first, we use the transfer matrix method to model the propagation through layers with a transmission matrix. The overall transfer matrix of the DBR is obtained by multiplying the matrices together. Then, from the transfer matrix, the reflectance of the DBR can be calculated. To employ the transfer matrix, one needs to investigate the electric(E) and magnetic(H) fields and their components at the boundary of two mediums. We refer to waves in the direction of incidence by a positive sign, and waves in the opposite direction by a negative sign.

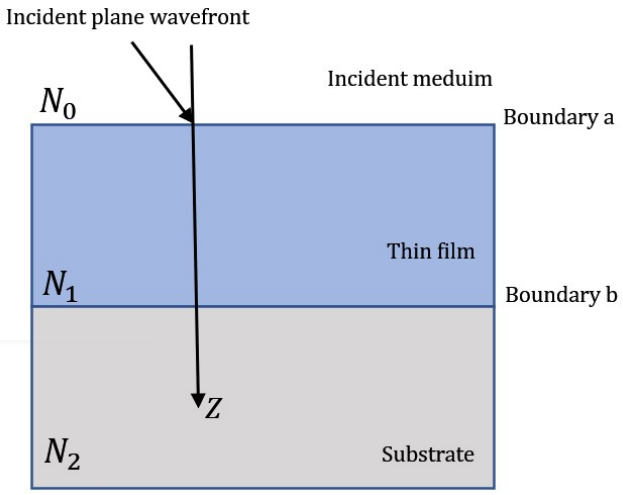

Figure 2.4. Plane wave incident on a thin film

The boundaries between the film and the incident medium and the substrate are shown by the symbols a, and b (Figure 2.4). By considering the tangential components of the fields and the fact that there is no negative-going wave in the substrate and the waves in the film can be introduced as one positive-direction wave and one negative-direction wave. At this boundary, then, the tangential components of E and H are[41]:

$$E_b = E_{1b}^{+} + E_{1b}^{-} \tag{2.7}$$

$$H_b = \eta_1 E_{1b}^{+} - \eta_1 E_{1b}^{-} \tag{2.8}$$

Where $\eta = \frac{H}{E}$ is optical admittance. Hence[41]:

$$E_{1a}^{+} = E_{1b}^{+} e^{i\delta} = \frac{1}{2}\left(\frac{H_b}{\eta_1} + E_b\right)e^{i\delta} \tag{2.9}$$

$$E_{1a}^{-} = E_{1b}^{-} e^{i\delta} = \frac{1}{2}\left(-\frac{H_b}{\eta_1} + E_b\right)e^{-i\delta} \tag{2.10}$$

$$H_{1a}^{+} = H_{1b}^{+} e^{i\delta} = \frac{1}{2}\left(H_b + \eta_1 E_b\right) e^{i\delta} \tag{2.11}$$

$$H_{1a}^{-} = H_{1b}^{+} e^{i\delta} = \frac{1}{2}\left(H_b - \eta_1 E_b\right) e^{-i\delta} \tag{2.12}$$

So that:

$$\begin{aligned} E_a = E_{1a}^{+} + E_{1a}^{-} &= E_b\left(\frac{e^{i\delta} + e^{-i\delta}}{2}\right) + H_b\left(\frac{e^{i\delta} - e^{-i\delta}}{2\eta_1}\right) \\ &= E_b \cos\delta + H_b \frac{isin\delta}{\eta_1} \end{aligned} \tag{2.13}$$

$$H_a = H_{1a}^{+} + H_{1a}^{-} = E_b\eta_1\left(\frac{e^{i\delta}-e^{-i\delta}}{2}\right) + H_b\left(\frac{e^{i\delta}+e^{-i\delta}}{2}\right) = E_b i\eta_1 \sin\delta + H_b \cos\delta \tag{2.14}$$

These two final Equations can be written in a matrix as

$$\begin{bmatrix} E_b \\ H_a \end{bmatrix} = \begin{bmatrix} \cos\delta & (i\sin\delta)/\eta_1 \\ i\eta_1 \sin\delta & \cos\delta \end{bmatrix} \begin{bmatrix} E_b \\ H_b \end{bmatrix} \tag{2.15}$$

The 2 × 2 matrix on the right-hand side of the Equation above is known as the characteristic matrix of the thin film. We can normalize this Equation by dividing through by Eb to give:

$$\begin{bmatrix} E_a/E_b \\ H_a/E_b \end{bmatrix} = \begin{bmatrix} B \\ C \end{bmatrix} = \begin{bmatrix} \cos\delta & (i\sin\delta)/\eta_1 \\ i\eta_1 sin\delta & \cos\delta \end{bmatrix} \begin{bmatrix} 1 \\ \eta_2 \end{bmatrix} \tag{2.16}$$

B and C are the normalized electric and magnetic fields.

This result can be immediately extended to the general case of an assembly of q layers when the characteristic matrix is simply the product of all matrices.

$$\begin{bmatrix} B \\ C \end{bmatrix} = \left\{ \prod_{r=1}^{q} \begin{bmatrix} \cos\delta_r & (i\sin\delta_r)/\eta_r \\ i\eta_r \sin\delta_r & \cos\delta_r \end{bmatrix} \right\} \begin{bmatrix} 1 \\ \eta_m \end{bmatrix} \tag{2.17}$$

Where η_r and η_m are the admittance of layers and substrate respectively.

The characteristic Matrix for a DBR with a Quarter Wavelength Design and optical thickness of π/2 (or its odd multiplies) becomes:

$$\begin{bmatrix} 0 & i/\eta \\ i\eta & 0 \end{bmatrix} \tag{2.18}$$

So, the reflectance of a DBR is[41]:

$$R = \left(\frac{\eta_0 B - C}{\eta_0 B + C}\right)\left(\frac{\eta_0 B - C}{\eta_0 B + C}\right)^{*} \tag{2.19}$$

where η_0 is the admittance of the incident medium. The abovementioned Equations are used in a MATLAB code to find the Reflection and validate the results of COMSOL[93]. The comparison of the reflection calculated by Equation 2.19 and the one which is obtained by the FEM method is presented in the results section.

2.1.4 Materials for DBRs

To achieve high reflectance, the contrast in the refractive index must be high (see Equation 2.3), there must be a low optical loss, and interfaces must be abrupt. Here, we will explain these three requirements. Higher contrast in the refractive index means more reflection occurs at each boundary as described before and as a result, higher reflectance[94] can be achieved with fewer DBR pairs. Furthermore, the stopband width is increased with larger contrast in refractive indices. Furthermore, the materials should have very low optical loss around the operating wavelength of the DBR because it can increase the absorption [32] and any significant absorption in the mirror will lower its reflectance (see Equation 1.6). Also, boundaries should be abrupt, and with little surface roughness because Fresnel Equations are defined for abrupt interfaces. In addition, the appreciable surface roughness of dielectric layers has been shown to increase absorption in dielectric DBRs[28-31]. Dielectric materials are electrical insulators and do not suffer from free-carrier absorption. As a result, they can have an extinction coefficient near zero. This is a huge benefit for DBRs to achieve high reflectance with low absorption. In this section, we will review some material properties of common DBR candidates to understand why they are used more.

TiO2 is a dielectric with a wideband-gap energy and high refractive index used in DBRs due to its optical properties. For instance, due to high transmittance and high refractive index in the visible region, it can be used in optical filters. TiO2 thin films can be fabricated using different techniques such as sputtering, sol-gel, pulse laser deposition, and electrodeposition[27].

MgF_2 has one of the lowest refractive index optical materials. This property, along with its low optical absorption, makes it an excellent choice for use in high-power laser systems[95].

Zinc sulfide, an important semiconducting material, has a wide optical band gap and high refractive indices. Its band gap energy has been found to increase as it goes from bulk to nano form, which makes it a potentially good material for reflective coatings [96]. ZnS has a high refractive index at the visible spectrum, a high dielectric constant at 1 MHz, and a wide wavelength pass band. Therefore it is useful for applications like filters, reflectors, and planar waveguides [97].

Tantalum pentoxide (Ta_2O_5) thin films have characteristics including a high refractive index, good thermal and chemical stability, and high optical transmission. It has a wide variety of applications such as protective coatings for optical filters, lenses, and even anti-reflection coatings. Ta_2O_5 films can be manufactured by various methods, e.g., ion beam sputtering, chemical vapor deposition, and RF sputtering [98].

Alumina (Al2O3) thin film has been widely used in many fields, especially in optical films and semiconductor industries, such as cavity coating, passivation or moisture barrier layer in solar cells, and protective layer. High melting point, good chemical stability, and compatibility with the semiconductor process are significant qualities for its applications. Al2O3 optical film has been prepared by different techniques based on the chemical vapor method and physical vapor methods, such as chemical vapor deposition, atomic layer deposition, and electron beam evaporation[99, 100].

These materials are all oxides, sulfates, or fluorides of different metals. The refractive index of mentioned materials in 700 nm and their melting point are gathered in Table 2.2. In our simulations SiO_2 is the choice for the low index of refraction material[101]. It offers a very low n of the dielectrics with reported values of n = 1.4622 and κ = 0.0014 at 700 nm. Since SiO_2 was chosen as the low refractive index material, TiO2 is a choice for the high index refraction material. It offers a high n of the dielectrics with reported values of n = 2.1126 and $\kappa = 0$ at 700 nm[102]. Therefore, a stack of SiO_2/TiO_2 at 700 nm has a contrast of:

$$\frac{\Delta n}{n} = \frac{n_{TiO_2} - n_{SiO_2}}{n_{SiO_2}} = \frac{2.83 - 1.45}{1.45} = 95\% \qquad (2.20)$$

This large contrast allows for the need for fewer pairs, a wider stopband, and a higher reflectance.

Table 2.2. some material properties of thin films[102].

material	Melting point (˚C)	Refractive index (700 nm)
SiO_2	1610	1.45
TiO_2	1858	2.83
Al_2O_3	2072	1.55
Ta_2O_5	1872	2.12
ZnS	1020	2.34
MgF_2	11266	1.42

2.2 Model and simulation

Electrical and magnetic fields are vector quantities that have both magnitude and direction. The relations and variations of the electromagnetic field, charges, and currents are governed by Maxwell's Equation and its differential form is the most applicable form to study boundary value problems. These Equations are defined below[103]:

$$\nabla \times H = \sigma E + \frac{\partial(\epsilon E)}{\partial t} \quad \text{Ampere's law} \tag{2.21}$$

$$\nabla \times E = -\frac{\partial(\mu H)}{\partial t} \quad \text{Faraday's law} \tag{2.22}$$

$$\nabla.(\epsilon E) = 0 \tag{2.23}$$

$$\nabla.(\mu H) = 0 \tag{2.24}$$

By using the curl of Faraday's law and substituting Ampere's law in it we obtain the governing Equation of the electromagnetic aspect of the structure.

$$\nabla \times (\mu^{-1}\nabla \times E) = -\frac{\partial(\nabla \times H)}{\partial t} = -\frac{\partial}{\partial t}\left(\sigma E + \frac{\partial(\epsilon E)}{\partial t}\right) \tag{2.25a}$$

$$\nabla \times (\mu^{-1}\nabla \times E) + \sigma\frac{\partial E}{\partial t} + \epsilon\frac{\partial^2 E}{\partial t^2} = 0 \tag{2.26b}$$

On the other hand, it is clear that because the plane wave $E = E_0 e^{i\omega t}$, hence, its first and second derivatives are:

$$\frac{\partial E}{\partial t} = j\omega E \tag{2.26}$$

$$\frac{\partial^2 E}{\partial t^2} = j^2\omega^2 E = -\omega^2 E \tag{2.27}$$

By substituting these two derivatives into Equation 26. b we obtain the governing Equation:

$$\nabla \times (\mu_r^{-1}\nabla \times \boldsymbol{E}) - \kappa_0^2\left(\varepsilon_r - \frac{j\sigma}{\omega\varepsilon_0}\right)\boldsymbol{E} = 0 \tag{2.28}$$

Here, μr denotes the relative permeability, j the imaginary unit, σ the conductivity, ω the angular frequency, εr the relative permittivity, and ε0 the permittivity of free space. The model uses material parameters for air as σ = 0 and μr = εr = 1 and SiO_2 and TiO_2 are defined by the library automatically. The refractive index is a wavelength-dependent variable and has different values. Hence, refractive indices for all materials need to be added as a table and the software uses them by defining an interpolation function between these values.

First, the reflectance of a Tungsten cube has been investigated in COMSOL by using a stationary solver as the physics is independent of the time. Calculation of reflectance requires a frequency domain for electromagnetic wave physic study, and thereby, the

‘Electromagnetic waves frequency domain’ is selected. This physic solves calculates the electric field from the Equation above[104].

Here, we modeled a 1000×1000×1000 nm cube that is subjected to an incoming electromagnetic periodic wave with 1.443×10-4[Watt] power which is explained in this part. The initial electromagnetic field in the model is 0 [v/m]. The environmental temperature and pressures are 293.15 K and 1 atm respectively. The schematic of the designed model is shown in Figure 2.5.

In this study, the source of light is a Gaussian laser beam which is incident on the top layer of the structure. The common image of a laser beam is a perfectly collimated beam of light with energy uniformly distributed across the cross-section of the laser beam. However, this is not an actual image of a laser beam propagation over any distance because diffraction causes the light waves to diverge transversely as they propagate (Figure 2.5). Electric field distribution for the gaussian beam is defined by[103]:

$$E(r,z) = \overrightarrow{E_0}\left(\frac{\omega_0}{\omega(z)}\right) e^{\left(\frac{-r^2}{\omega^2(z)}\right)} e^{i\left(kz-\eta(z)+\frac{kr^2}{2R(z)}\right)} \tag{2.29}$$

where $r = \sqrt{x^2 + y^2}$ is the transverse distance from the central axis, η is the wave impedance of the medium in which the beam is propagating, $\omega(z)$ is beam radius and defined[93, 103]:

$$\omega(z) = \omega_0\left(1 + \frac{z^2}{z_0^2}\right)^{1/2} \tag{2.30}$$

and ω_0 is the beam radius at the waist and is obtained by:

$$\omega_0 = \frac{\lambda}{\pi\theta_0} \tag{2.31}$$

and R(z) is wave front:

$$R(z) = z\left(1 + \frac{z_0^2}{z^2}\right)^{1/2} \tag{2.32}$$

Irradiance is the power carried by the beam across a unit area of cross-section of the beam (W/m^2), and its profile is not necessarily uniform and is given by a Gaussian function:

$$I(r,z) = \frac{|E(R,Z)|^2}{2\eta} = I_0(\frac{\omega_0}{\omega(z)})^2 e^{(\frac{-2r^2}{\omega^2(z)})} \tag{2.33}$$

Then the intensity at the center of the beam waist can be written as:

$$I(r) = I_0 e^{(\frac{-2r^2}{\omega_0^2})} = \frac{2P}{\pi\omega^2} e^{\frac{-2r^2}{\omega_0^2}} \tag{2.34}$$

Where P is the total power in the beam. On the center axis r =0 and $I=I_0$ such as:

$$I_0 = \frac{2P_0}{\pi\omega_0^2} \tag{2.35}$$

Maintain properties of such a source are wavelength (or frequency), Power of the beam, divergence angle of the beam (θ_0), and beam waist radius (ω_0). A Gaussian beam has a waist, where the ω_0 is the narrowest one. It diverges from this beam waist and this divergence is recognized by the angle θ which is subtended by the points on either side of the beam axis where the irradiance has dropped to $1/e^2$ of its value on the beam axis, this is the place where the electric field has dropped by 1/e[89].

There are various types of laser beams available for different applications operating near the 700 nm range. Some examples of these beams providing different powers are mentioned in Table 2.3 and as you see the power varies between the values less than 1 and up to 100 mWatt[93]. Hence, we can define our laser characteristics based on available ones. Here, we assumed a laser with 700 nm wavelength, a divergence angle of 0.00075 radians, and a power of 0.2 Watt.

So, for the chosen laser beam, the beam waist is given as:

$$\omega_0 = \frac{700 \times 10^{-9}}{\pi \times 0.00075} = 297.089 \times 10^{-6} \quad [m] \tag{2.36}$$

Now, one can calculate the intensity of the source based on its power and beam waist radius as follows.

$$I_0 = \frac{2 \times 0.2}{\pi(297.089 \times 10^{-6})^2} = 1.443 \times 10^6 \ \left[\frac{W}{m^2}\right] \tag{2.37}$$

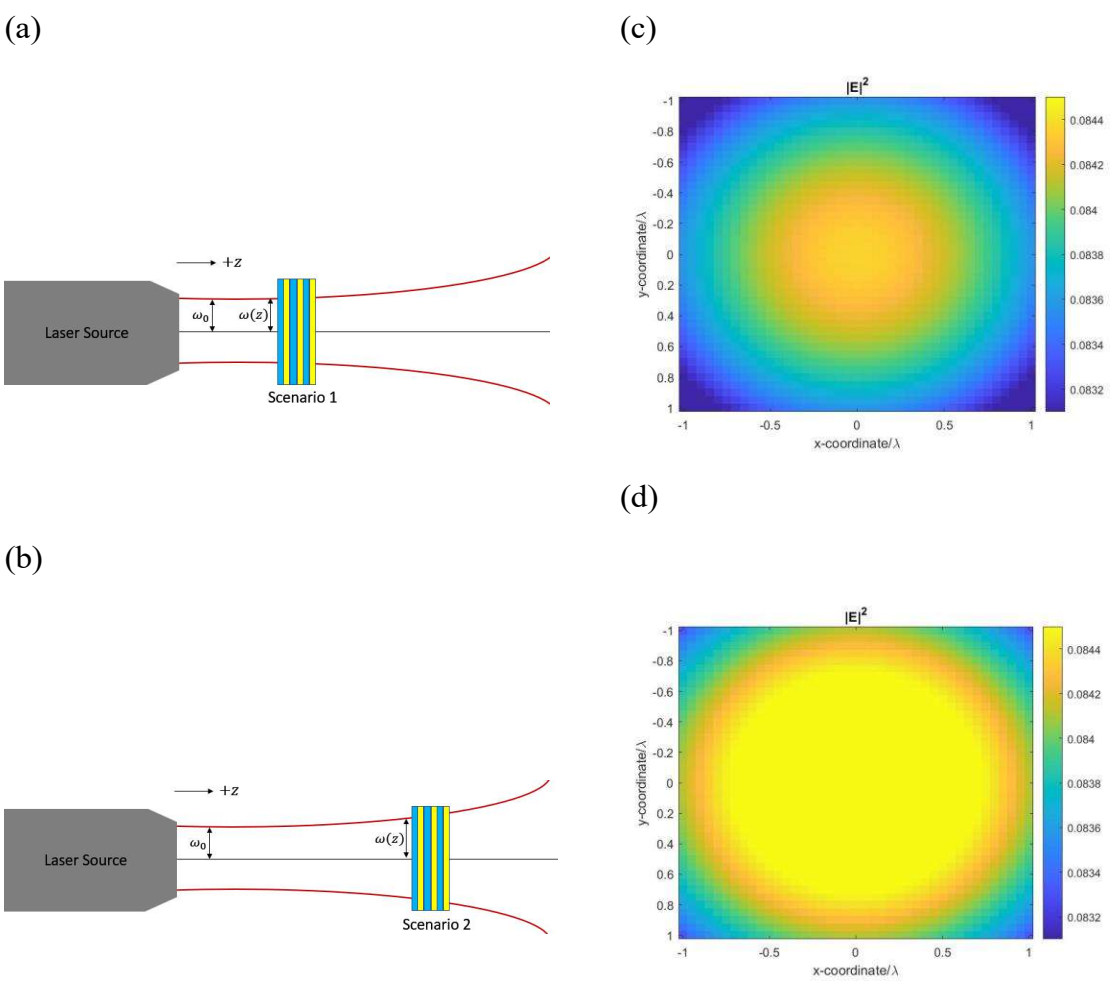

Figure 2.5. Schematic of a multilayer structure exposed to a Gaussian laser beam at different locations along the propagation axis (a) Scenario1 at $\omega(z)=1.01\times\omega(z0)$, and (b) Scenario2 at $\omega(z)=\sqrt{2}\times\omega(z_0)$, Electric field intensity distribution of the incident light for (c) Scenario 1, and (d) Scenario 2.

Table 2.3. available commercial laser devices operating at wavelengths near 700 nm[93].

Wavelength (nm)	type	Output power (mW)	Beam divergence (mRad)	Laser name
635	diode	25	<0.001	Red and IR Alignment
680	diode	4.9	0.0007	Circular Beam Visible
660	diode	80	<0.001	S3-Series Laser
655	diode	10	<0.001	Red and IR Alignment
635	diode	100	<0.001	Red and IR Alignment
665	diode	0.9	0.7	Circular Beam Visible
685	diode	50	NA	Fiber-Coupled
700	diode	50	NA	QLD-700-50S
700	diode	20	NA	QFLD-700-20S

Power is independent of the cross-section area value, but the intensity is a dependent value with regard to area. Hence, one needs to transform the power of the source into the power which affects the object by multiplying the intensity by the surface area of the object. A typical intensity distribution of the laser beam is plotted in Figure 2.5, where the intensity distribution is given for two different scenarios at different locations along the z-axis. In reality, the dimension of a unit cell of the model is smaller than the beam waist, So, it should be considered in the power calculation.

$$P = I_0 \times A \tag{2.38.a}$$

$$P = 1.443 \times 10^{6} \times 1 \times 10^{-6} \times 1 \times 10^{-6} = 1.443 \times 10^{-6} \quad [W] \tag{2.39.b}$$

This is the power that we defined in COMSOL as input power.

In Figure 2.5, for scenario 2, the incident angle of laser beam deviates slightly from the normal line. The divergence angle of the laser beam is 0.00075 radians (0.04 degrees), which has a small effect on the reflectance in the calculations. In Figure 2.6, the effect of beam divergence angles between 0.01 and 0.05 degrees on the maximum temperature of the structure is demonstrated. As it is shown on the figure, the maximum

temperature of the structure decreases only 0.09 K by increasing the incident angle from 0 to 0.05 degrees which is neglectable compared to the temperature increment in the multilayer structure.

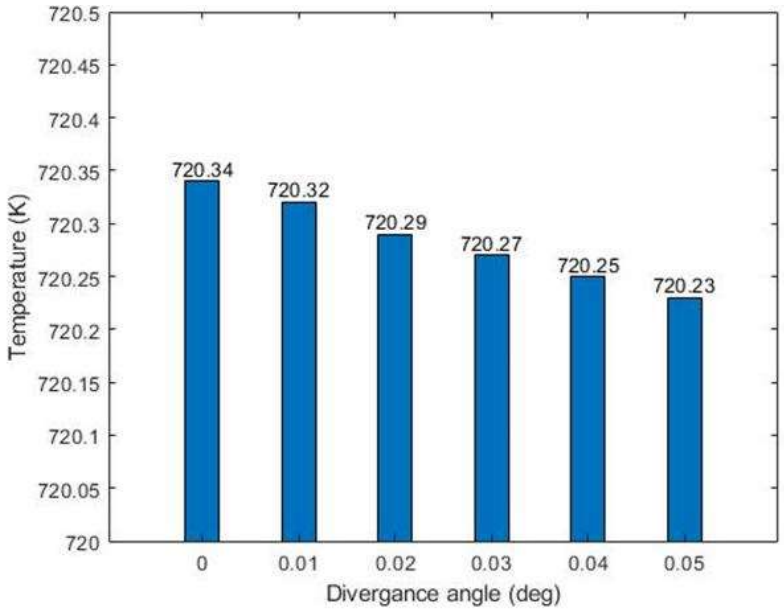

Figure 2.6. The effect of the divergence angle of the laser beam on the maximum temperature

Figure 2.7 illustrates the uncoated (left) and coated (right) Tungsten with 10 layers model. The same simulation can be done for the different number of layers. The thickness of coating layers is obtained by Equation 2.7.

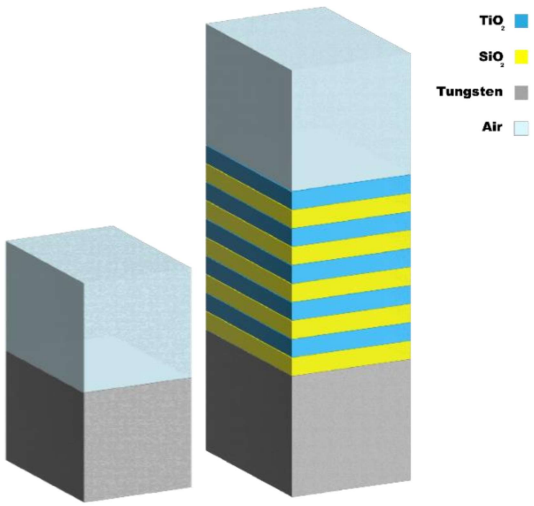

Figure 2.7. the schematic of the COMSOL model for coated and uncoated substrate

We can assume periodic boundary conditions on the walls which means the condition at the walls are the same and continuous[104]. This boundary condition makes the electric field periodic (being equal to the source and destination). The boundary condition on the bottom wall is assumed to be insulation. The mesh that is applied is a tetrahedral mesh with maximum and minimum element sizes of 150 and 100 nm and a maximum element growth rate of 1.5.

In the next part, the effect of different factors on the reflectance of the structure is investigated and results are reported.

2.3 Results and discussions

Before applying any coating to improve the surface reflection of the Tungsten, there should be a study on the reflectance of this metal to consider it as a reference so one can make a comparison between this result and any further efforts for enhancing it. The result for the absorptance, transmittance, and reflectance versus frequency for an uncoated Tungsten conducted in COMSOL is shown in Figure 2.8.

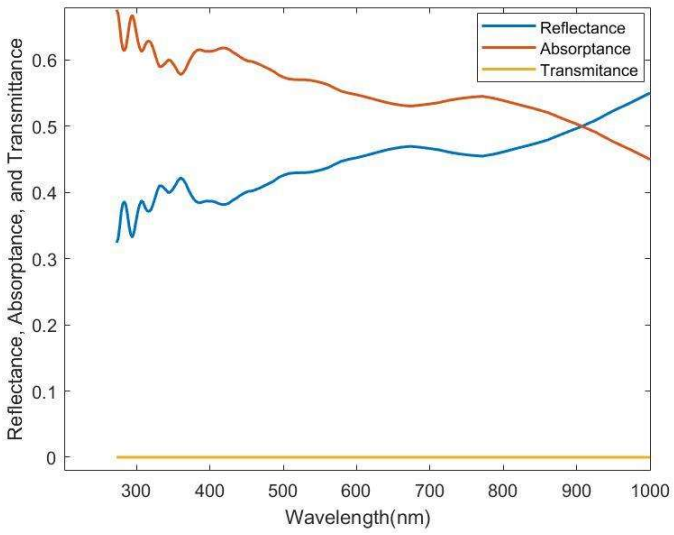

Figure 2.8. Reflectance, absorptance, and transmittance of uncoated Tungsten

As one can see, the sum of reflectance and absorptance is equal to one and the reflectance quantity for frequencies between 300 and 1000 nm is in the range of 0.33 up to 0.55. Generally, the value of reflectance increases by increasing the wavelength in this range, but for the design wavelength (700 nm) it is about 0.45. To be more specific, Tungsten absorbs about half of the energy that it receives from the incident laser beam. Therefore, this reflectance should be increased by adding low-index and high-index periodic layers to decrease the surface absorption in the Tungsten so avoiding unwanted heat transfer in the medium becomes possible. In what follows, we are going to investigate the effect of adding these layers to the substrate on the reflectance and temperature of the structure.

Adding multilayer impact

As mentioned before, one way to increase the reflection is by using DBRs on top of the refractory metals. Here, we added 6 layers of alternating SiO_2 and TiO_2 layers as low-index and high-index materials to investigate the reflectance increment. The thickness of the layers is defined as 50 nm randomly and without any calculation. The effect of thickness optimization on the reflectance enhancement will be studied in the next step. A comparison of the reflectance in the model without and with six added layers is shown in Figure 2.9.

As it is obvious, reflectance has been increased significantly for the wavelengths between 370- 712 nm (frequencies 800-421 THz), and the maximum value has reached 0.9. It means that by modifying the thickness and the number of layers we can improve the reflectance for specified frequencies. However, this improvement is not dominant for the desired frequency (700 nm) but the 500 nm and this is rational because of the random thickness choice. We expect to be able to adjust this peak on the wavelength of 700 nm by using calculated thicknesses in the next part.

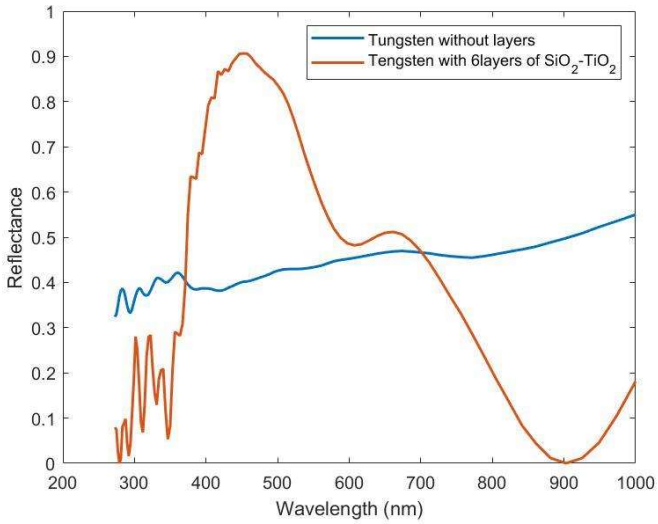

Figure 2.9. The effect of adding 6 layers of coating on top of the Tungsten substrate on Reflectance

Thickness optimization impact

As shown in the previous part (Figure 2.9), there is a zone in which the reflectance is very high. The location of such a high-reflection zone in the spectrum is modified by optimizing the thicknesses of the periodic layers of DBR[33, 36, 105].

From Equation 2.7, assuming that the target wavelength is 700 nm, and the fact that the angle of the incident wave is zero at the boundary, we can find the thickness of the layers. Table 2.4 shows the refractive indices at 700 nm and calculated thickness for different materials used in DBRs by employing Equation 2.7.

The complex refractive index of Tungsten[106], SiO_2[102], and TiO_2[102] are dependent on the wavelength and are defined as a table in COMSOL. The values of the n at 700 nm for SiO_2 and TiO_2 layers are 1.4553 and 2.83 respectively, and the values of the imaginary part k at 700 nm for SiO_2 and TiO_2 layers are zero. Also, it is mentioned before that the optical thickness in this formula should be set to $\pi/2$ to make a π phase shift[41]. The reason is to make all of the reflected beams from the layers constructive, thereby we make a total reflected beam as a summation of all of the beams and can reach the maximum reflection. By using the mentioned Equation, we determine the thickness of SiO_2 and TiO_2 layers equal to 120 and 62 nm, respectively (as

mentioned in Table 2.4). The comparison between the reflectance of an optimized and non-optimized thickness layered structure is depicted in Figure 2.10. Table 2.5 shows a comparison between the value of the reflectance at 700 nm for the structure before and after thickness optimization.

Table 2.4. Optimized thicknesses for different materials based on Equation 2.7.

material	n	k	d (nm)
Ta_2O_5	2.124	0	82
TiO_2	2.830	0	62
MgF_2	1.420	0	124
SiO_2	1.453	0	120
Al_2O_3	1.755	0	100
ZnS	2.347	0.031	74

Table 2.5. Effect of thickness optimization on the average Reflectance

Reflectance for 400-500 THz (around 700nm)	
Before thickness optimization	0.46
After thickness optimization	0.79
Percentage of reflectance increase	72%

From table 2.5, as one can see, although our aim in this part was to adjust the location of the center wavelength of the reflectance curve and not increase its value of it, we could enhance the reflection by about 72% by adjusting the thickness of the layers.

As we expect, the reflectance peak is closer to 700 nm and the high reflectance region has been wider now (Figure 2.10). The center of the high reflection zones shifted to slightly lower wavelengths (650 nm) because of the interference with the Tungsten (W) at the bottom and it can be improved by increasing the bandwidth in the next step. It can be seen that the bandwidths of the high-reflectance zones for these individual designs are low because we designed them for one specific wavelength. To increase the

bandwidth, there are two solutions. First, we can apply several periodic segments adjusted for different wavelengths and stack them on top of each other[14]. Moreover, we can increase the bandwidth by increasing the number of periodic layers in a specific DBR[107]. In the next part, we are going to apply the latter method to overcome the current problem.

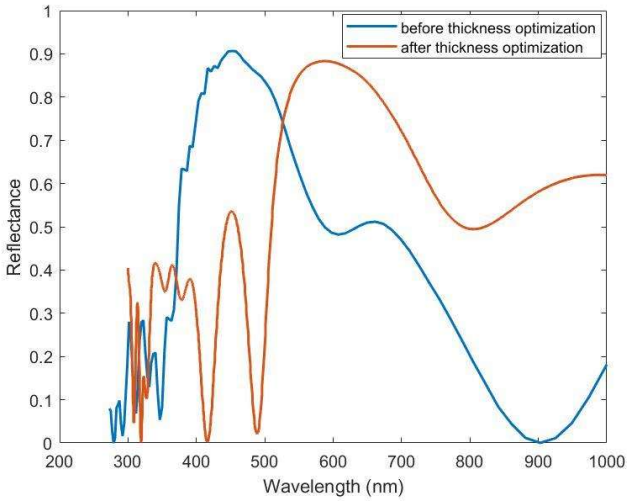

Figure 2.10. The effect of thickness optimization on Reflectance of SiO_2, TiO_2 multilayers

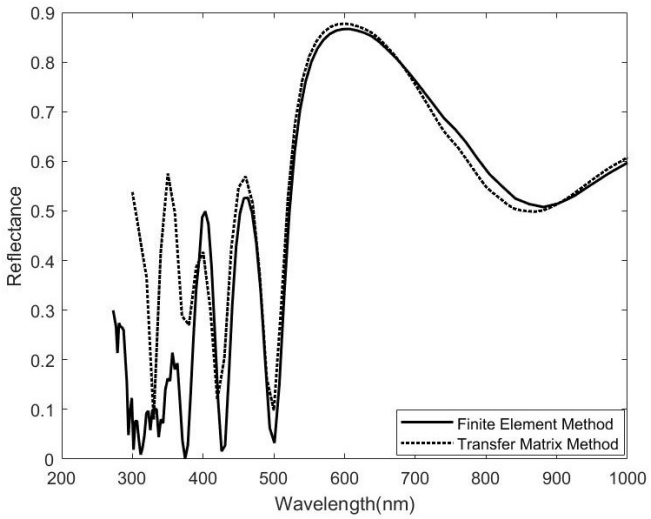

Figure 2.11. The comparison of the Finite Element and Transfer Matrix methods

The comparison of the FEM results and TMM results are given for a Tungsten substrate coated with 6 layers of SiO_2 and TiO_2

in Figure 2.11. The results agree well, and similar reflection is obtained over the spectrum of interest.

Impact of the number of layers

In the previous step, we succeeded in moving the peak of the reflectance curve closer to the design wavelength but could not adjust it accurately. Also, the bandwidth of the design is narrow so if the input laser beam wavelength changes slightly the reflectance value may drop significantly. One of the main factors to enhance the bandwidth of high reflectance area is the number of layers stacked to the refractory metal substrate[27, 107, 108]. The more layers that are added, the higher the resulting reflectance will be. In addition, the reflections should all be in phase with each other to get constructive interference. The effect of the number of segments is investigated by adding more high-index and low-index pairs on top of the Tungsten. The result of using 6, 8, 10, and 12 layers in the DBR is depicted in Figure 2.12.

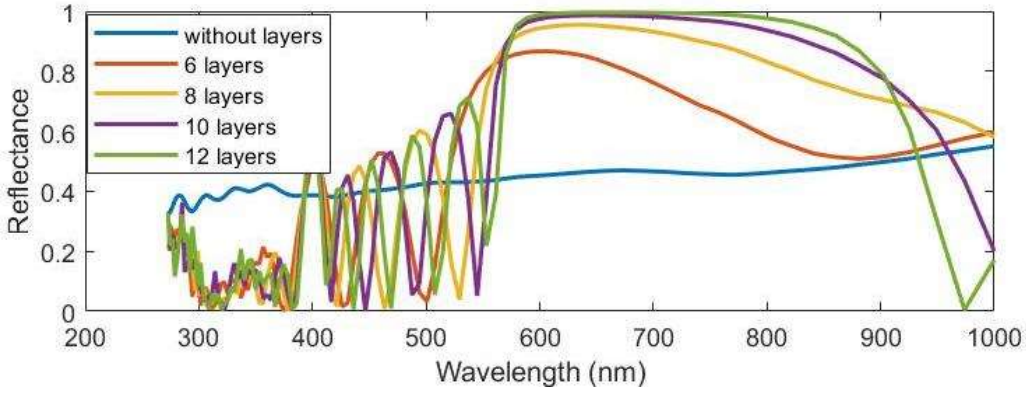

Figure 2.12. The comparison of the Finite Element and Transfer Matrix methods

From Figure 2.12, the overall behavior of the curves remains the same as we expect for example there is a huge drop for the wavelengths below 600 nm and there are several

dips and fluctuations in this area. However, the bandwidth of the high reflectance regime has been increased for wavelengths around 700 nm by increasing the number of layers. Also, there is a considerable enhancement in the maximum reflectance in each curve. The maximum value of the reflectance has been increased up to 0.99 for 12 layers of coating. The high reflectance (above 0.8) bandwidth for 6, 8, 10, and 12 layers are in the range of 522-686, 544-822, 553-881, and 561-902 nm, respectively. In other words, the bandwidth increased from 164 nm to 341 nm, which means about 100% improvement by increasing the number of layers from 6 to 12. However, the bandwidth difference between the 10 and 12 layers of coating is just 13 nm. To discuss more specifically, increasing from 6 to 8 layers makes more significant changes but this improvement rate slows down for a greater number of layers. There is a very slight change after 10 layers. As a result, we selected the number of layers as 10 for thermal calculations. A comparison between the reflectance value at 700 nm for a various number of layers is summarized in Table 2.6.

Table 2.6. Effect of the number of layers on the average Reflectance

Reflectance for 580-840 nm (around 700nm)	
6 layers of coating	0.75
8 layers of coating	0.90
10 layers of coating	0.96
12 layers of coating	0.99
Percentage of reflectance increase of 12 layers compared to 6 layers	32%

To conclude, by designing the number and thickness of SiO_2 and TiO_2 thin-film layers, the average reflectance for frequencies near 700 nm has been enhanced from 0.46 to 0.99, which means an 115% increase in the reflectance value. As a result, we expect that the energy absorbed in the structure with 10 layers of coating will decrease significantly because absorption decreases to 4% when the reflection increases to 96%. The thermal balance of a structure in an environment is strongly dependent on thermal emission from the structure's surfaces. Therefore, an estimation of the emission of the DBR coating on the provides a perspective of the resultant thermal curves. Table 2.7 illustrates that emittance decreases significantly as the number of layers increases. So,

we expect the temperature to decrease by increasing the number of layers as the absorption decreases.

Table 2.7. Effect of the number of layers on the emittance at 700nm

Number of the layers	Emittance
No layers of coating	0.55
6 layers of coating	0.25
8 layers of coating	0.1
10 layers of coating	0.04
12 layers of coating	0.01

In the next part, we will study the importance of the materials that are used for coating and make sure the selected materials are the best choice for the aim of this research.

Material choice comparison

One of the most important factors in multilayer design is material selection. As one may expect, in low-index and high-index multilayers, the efficiency of the structure increases by increasing the difference between two successive layers' refractive index. On the other hand, the other criteria in the material selection is posing a lower thermal conductance of the structure. So, here we have compared both reflection changes in the structures for 10 layers of coating. Since we concluded that the coating composed of 10 layers with the aforementioned calculated thicknesses holds the maximum efficiency among the other models, in this part we do not change any other variable and just alter the materials. The comparison of reflectance between various materials chosen for the same design is shown in Figure 2.13.

As is shown in Figure 2.13, the worst case happens for a Tungsten without any DBR on top of it. The reflectivity over desired wavelengths (around 700 nm) is over 98% for SiO_2/ TiO_2 and MgF_2/ TiO_2 structures and has been improved by around 96% in comparison to the structure without any multilayer coating (made of a Tungsten cube). Any other combination of low-index and high-index materials lies under them. This is exactly what is expected due to the smaller difference between the refractive indices of

two successive materials. The difference between the SiO_2/ TiO_2 and MgF_2/ TiO_2 combinations is negligible, thereby there is no need to change the materials in our previous designs and we will investigate the thermal studies on the same structure in the next chapter.

The incident angle is an important factor in studying the light reflected from the surface. Figure 2.14 illustrates the reflectance spectrum for different angles of incidents varying from 0 to 40 degrees. The proposed structure in this study is designed for 0 degrees, and by increasing the incident angle 3 dips arise one of them is around our target wavelength. Based on the results, the best angle of the incident to achieve maximum reflection is 0 degrees. In low-index and high-index multilayers, the efficiency of the structure increases by increasing the difference between two successive layers' refractive index.

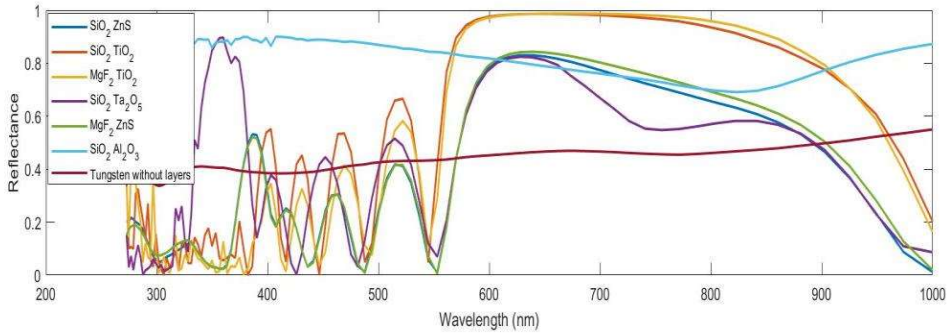

Figure 2.13. The comparison of the effect of the material choice on reflectance

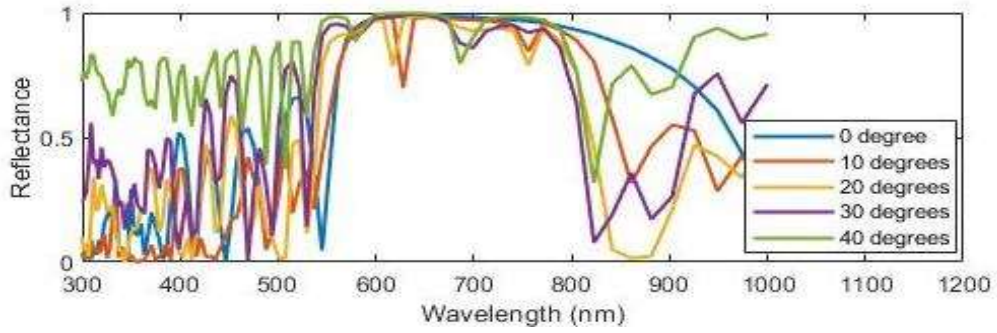

Figure 2.14. The comparison of the effect of the angle of incidence on the reflectance

In conclusion, the reflectivity from the surface of the refractory metal has been increased by the advantage of implementing a DBR on the top surface of the metal which was exposed to the incident light. This enhancement has been studied by varying different factors such as thickness, number, and material choice of the layers. The highest efficiency is achieved by using alternating high-index and low-index 10 layers of SiO_2/ TiO_2 thin films with thicknesses of 120 and 62 nm respectively. With regard to the mentioned design the reflectance of the whole structure has been increased from 0.46 to 0.96, which represents a 108% improvement. Also, the proposed structure in this study is designed for 0 degrees, and by increasing the incident angle 3 dips arise one of them is around our target wavelength. Based on the results, the best angle of the incident to achieve maximum reflection is 0 degrees.

3. A THERMAL STUDY ON DECREASING THE TEMPERATURE IN REFRACTORY METALS SUBJECTED TO AN ELECTROMAGNETIC WAVE BY SPECTRALLY SELECTIVE THIN-FILMS FILTER

Temperature discernment of a design is crucial in many aerospace, industry, and laser-related technologies. As discussed in chapter 2, refractory metals such as Tungsten absorbs most of the incident light due to its relatively low reflectance in 300-1000 nm wavelengths. As a result, the temperature increases inside the metal and can lead to the failure of the whole structure. To overcome this issue, we considered the implementation of Distributed Bragg Reflectors to control the temperature by decreasing the absorbed energy. As it is illustrated in Figure 2.1, the incident light to the surface of a multilayer structure is divided into two parts. The first part is reflected, and the rest is absorbed due to the electromagnetic losses of the material. By using DBRs, the reflection part that is transferring heat to the environment by radiative heat transfer has been enhanced and this leads to less absorption of the incident light. Nevertheless, the absorbed portion travels in the structure via the conductive heat transfer which leads to the temperature rise and is still necessary to be considered.

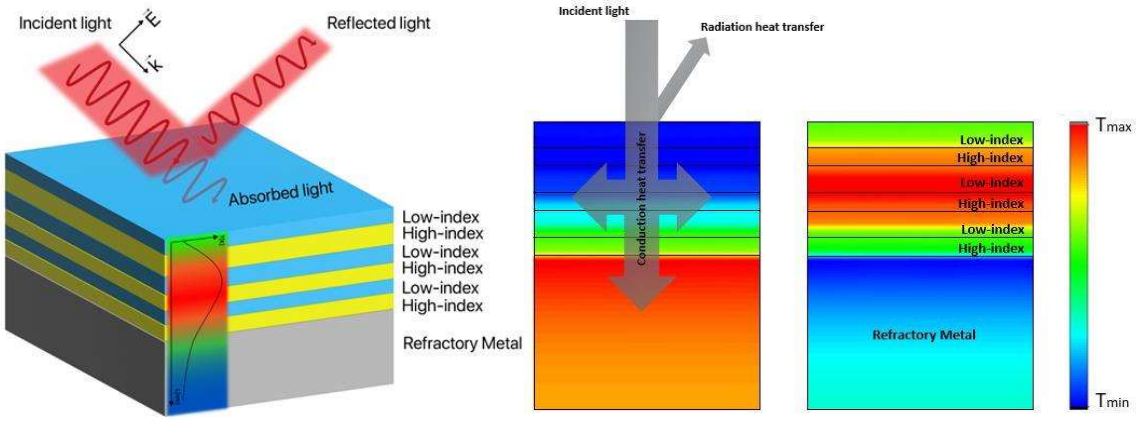

Figure 3.1. A schematic of temperature distribution in a refractory metal and a DBR structure on top of that and the heat transfer mechanisms participating in the energy balance of the structure.

In this chapter, the objective is to study the thermal merits of using DBRs in reducing temperature and investigating the behavior of the temperature change during the time.

3.1 Methodology

As mentioned before, the main objective of this study is to decrease the maximum temperature of the structure. This increase in the temperature is caused by the absorption of the incident light and propagation of the electromagnetic field in the object. Therefore, combining the electromagnetic studies with the heat transfer investigations is essential to have a general view of the mechanisms that are governing the heat and energy transferred in the multilayer structure. In the previous chapter, we studied the effect of different factors on reflectivity, and here our aim is to make a conclusion about the effect of these materials on the temperature. The very first step in finding the maximum temperature of the structure is understanding the Fourier Heat Transfer Equation. The general formulation of the heat transfer in the structure is based on the energy conservation law. Based on this law, the total energy of an isolated system remains constant at each time. In other words, the total incoming energy to any volume is equal to the summation of transferred outgoing energy and the amount of internal energy increment of the volume. The right-hand side of Equation 3.1 represents the incoming energy that is produced by the incoming electromagnetic field. The first expression in the left-hand side of the Equation represents the internal energy change of the structure and the second term is the energy that is transferred by conductivity[109, 110].

$$\rho C_p \frac{\partial T(x,y,z,t)}{\partial t} - k\,\nabla T(x,y,z,t) = Q(x,y,z,t) \tag{3.1}$$

$\rho, k,$ and C_p are mass density, thermal conductivity coefficient, and heat capacity at constant pressure. Furthermore, the convection heat transfer from the top surface plays an important role in cooling the structure and is defined as a boundary condition on the

very top surface. In this study, we considered the structure to be composed of a thin-film layer, and we applied a piecewise homogenous media, where the material properties of each layer are constant within each layer. As a result, we assumed the material properties, ρ, C_p, and k, are constant within a layer for each material.

In this study, $Q(x,y,z,t)$ is generated by electromagnetic losses within the layers which are affecting the structure. This electromagnetic loss is given as:

$$Q(x,y,z,t) = Q_{rh}(x,y,z,t) + Q_{ml}(x,y,z,t) \tag{3.2}$$

Where Q_{rh} and Q_{ml} represent resistive losses and magnetic losses respectively and are defined as[103, 111]:

$$Q_{rh}(x,y,z,t) = \frac{1}{2} Re(J(x,y,z,t).E^*(x,y,z,t)) \tag{3.3}$$

$$Q_{ml}(x,y,z,t) = \frac{1}{2} Re(i\omega B(x,y,z,t).H^*(x,y,z,t)) \tag{3.4}$$

Where ω, J, E, B, and H are frequency, current density, electric field, magnetic flux density, and magnetic flux, respectively. These quantities can be position and time-dependent; However, in this work, they are not changing over time, and we solve them with a stationary solver. ω is the frequency of the input electromagnetic wave. In this study, we considered a 700nm laser beam that corresponds to 428 THz.

3.2 Model and simulation

In continuous of our previous design, the same structure has been simulated in COMSOL[93] by using ELECTROMAGNETIC HEATING Multiphysics and implementing heat transfer in solid and electromagnetic-frequency domain physics for the thermal and electromagnetic investigations respectively. one can assume periodic boundary conditions on the side walls which means the condition at the walls are the

same and continuous (for example, the temperatures on these boundaries are equal). The boundary condition on the bottom wall for the thermal part is assumed to be convection. Furthermore, the radiation heat transfer from the top surface to the ambient plays an important role in cooling the structure and is defined by heat flux boundary condition on the very top surface by equation 3.5.

$$Q(x,y) = \sigma\varepsilon(T^4 - T_{am}^4) \tag{3.5}$$

Where $\sigma, \varepsilon,$ and Tam are Stefan's constant (5.67×10^{-8} Watt/m^{2}K^4), emissivity, and ambient temperature (293.15 K). The emissivity is defined as the average absorbance in a broadband spectrum. The absorptance graphs are obtained in the electromagnetic study for all of the structures, and the average of these values are tabulated in Table 3.1 and are used to calculate the radiation heat flux from the top surface to the environment. A basic thermal model description with estimated heat loads provides a better context for thermal analysis and the results and temperatures. A diagram with thermal and radiation loads, and boundary conditions has been shown in Figure 3.2.

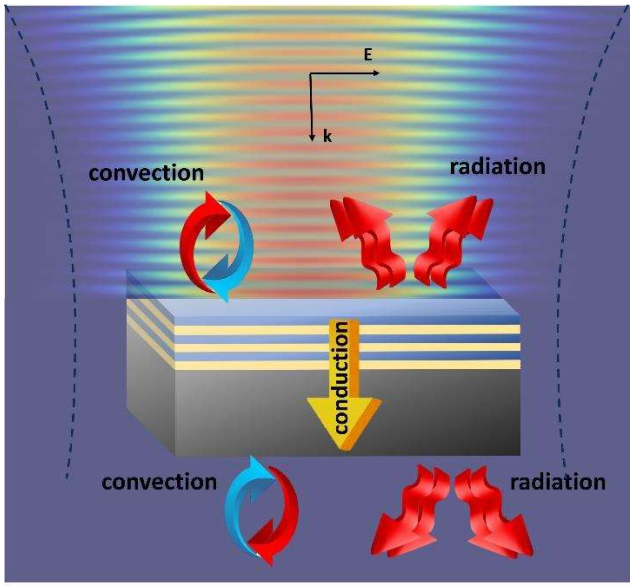

Figure 3.2. A schematic of the thermal loads and boundary conditions of the design

The electromagnetic wave is defined as the previous one by choosing the top and bottom surfaces as input and output (Port 1 and Port 2) and the input power. Here, to obtain more detailed and accurate results, three various power quantities are chosen and named high, medium, and low power which will be discussed in the next section.

Table 3.1. the emissivity of different materials in a 10-layer DBR obtained from the absorptance curves.

Material	emissivity
Ta_2O_5 / MgF_2	0.630
TiO_2 / SiO_2	0.586
TiO_2 / MgF_2	0.567
SiO_2 / ZnS	0.693
SiO_2 / Ta_2O_5	0.615
Al_2O_3 / SiO_2	0.203
MgF_2 / ZnS	0.687
Al_2O_3 / TiO_2	0.120

The incident wave is defined as a periodic wave with an incident angle of zero which means perpendicular to the surface. Initial temperature and pressures are 293.15 K and 1 atm. Important material properties used in this model are defined in Table 3.2.

Table 3.2. Important material properties used in heat transfer modeling in COMSOL.

Material properties	SiO_2	TiO_2	Tungsten
Thermal conductivity [W/m.K]	1.1	1.3	174
Mass density [Kg/m^3]	2300	4000	19350
Heat capacity (Cp) [J/Kg.K]	713	680	132

3.3 Results and discussions

In this section, the effectivity of two key factors on the temperature of the structure versus time is examined. These two factors are the number of DBR layers and material selection that are studied separately for different power values. Therefore, detecting the maximum temperature of the structure during the time and evaluating its behavior has been feasible in this section.

Impact of the number of layers

As discussed in chapter 2, the number of DBR layers plays an important role in the efficiency of the structure. In the previous chapter, we studied the effect of this factor on the wave reflection aspect. Now, the mentioned factor's impact on the maximum temperature is investigated to be compared with the counterpart result for the reflection study to accomplish an optimized number of layers for the DBR. The research is conducted for two different values for the power named high and low power, so, it is possible to compare the trends of Temperature versus time curves with regard to the magnitude of the input power. These powers are selected from a range of available red lasers and their magnitudes are 200 mW, 1.38 mW, and 0.13 mW. It is worth mentioning that these are namely powers, and according to Equations 2.36-2.39, the actual input powers for this design are 1.443×10-6, 1×10-8, and 1×10-9 watts, respectively. The results of this simulation are depicted in Figure 3.3.

As a result of reflectance increasing by adding more coating layers, we expect less energy and conductive heat conveyed into the structure. Hence, the temperature of the substrate should decrease as can be seen in Figure 3.3. The temperature reduction for both high and low powers is considerable as it is about 1300 and 20 K in comparison to the Tungsten without a coating, respectively. Thereby, using DBRs is an efficient way to reduce the temperature in refractory metals such as Tungsten. It is worth mentioning that in the low power case, the effectiveness of adding more layers decreases for more than 8 layers, and the temperature of 10 and 12-layer coatings are close enough to Figure out that there is no need to investigate multilayers with more than 12 layers unless the problems in which any small amount of temperature decrements is crucial.

It can be concluded that according to the previous results from chapter 2 and Figure 3.3.b, choosing 10 layers of coating is appropriate for a low power value. Nevertheless, the temperature increase for high-power case is relatively notable and the maximum difference between a model with 10 and 12 layers of coating is about 200 K.

Another interesting outcome in Figure 3.3 is the time constant of the curves. The time constant is a dimensionless value that represents the time in which the curve's behavior changes from transient to stationary. This time for the low power case is 0.3 seconds and unvaried by changing the number of layers. However, for the high-power case, this time increases from 0.01 to 0.21 by increasing the number of layers and it is not constant for

all designs. The change in this time constant from low-power laser to high-power laser is a result of the nonlinearity of the system, as the radiation heat transfer mechanism in high laser power becomes more dominant. As is shown in the model and simulation part, the only nonlinear governing equation in the system is radiation heat flux on the top surface which is a function of the fourth power of the temperature. In high-power cases, radiation plays a more important role in the thermal aspect and the relevant nonlinearity becomes more dominant. Also, the curves are sharper, and this confirms the fact that the radiation heat transfer is dominant for higher powers and temperatures and compensates for the absorbed energy in a shorter time. Our simulations confirm the abovementioned statement by representing the radiation heat transfer percentages as 1.5%, 4%, and 32% of the total heat transfer for low, medium, and high-power quantities, respectively. Although we did not present the results for much higher powers it is worth mentioning that by increasing the power value the radiation heat transfer mechanism contribution increases up to 50% for a sample power of 2 Watts.

It can be concluded that choosing 10 layers of coating is sufficient for low laser power. Nevertheless, the temperature increase for high power cases is relatively notable and the maximum difference between a model with 10 and 12 layers of coating is about 300 K. However, by using 10 layers of coating, 85% of the efficiency of 12 layers is achieved. In summary, the enhancement of 6% and 457% is achieved by adding 12 layers for low and high powers, respectively. In the following part, the effect of material choice on the efficiency of a DBR with 10 layers will be discussed.

(a)

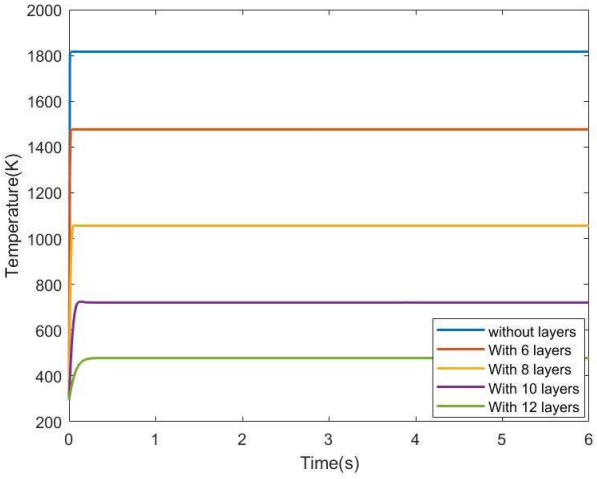

(b)

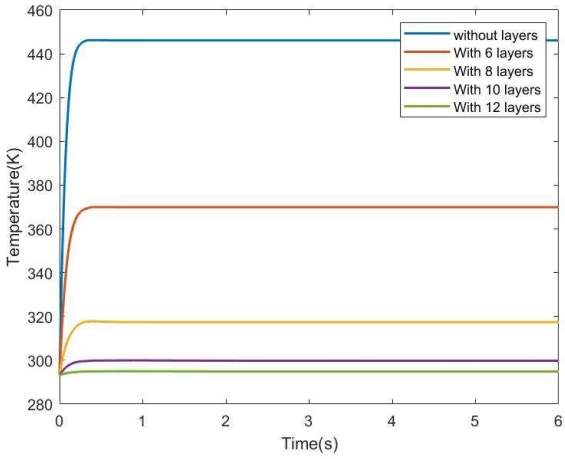

(c)

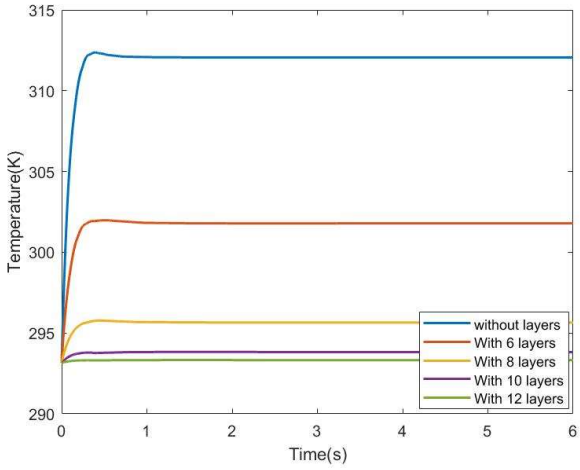

Figure3.3. Temperature variation during the time for the input power of (a) 1.443×10^{-6} (b) 1×10^{-8} (c) 1×10^{-9}

Material comparison for 10 layers

An important factor to study in this survey is the effect of material choice. In chapter two, the effect of material choice on reflectance is discussed. Up to this point, 10 layers of SiO_2-TiO_2 multilayer on top of the Tungsten is the optimum model. In this part, we will investigate the impact of material choice on decreasing the maximum temperature of the structure.

The study is conducted for three different values for the power named high, medium, and low powers, so, it is possible to compare the trends of Temperature versus time curves with regard to the magnitude of the input power. These powers are selected from a range of available red lasers and their magnitude are 200 mWatt, 1.38 mWatt, and 0.13 mWatt. As mentioned in the previous part, these are namely powers, and according to Equations 2.36-2.39, the actual input powers for this design are 1.443×10^{-6}, 1×10^{-8}, and 1×10^{-9} watts, respectively. The results of this simulation are depicted in Figure 3.4. In conformity with the reflectance study result (Figure 2.12), it can be observed that the abovementioned structures (SiO_2/TiO_2 and MgF_2/TiO_2) have the best thermal results and less transportation of heat through the structure due to less absorption and more reflection.

As a result of studying the material's effect on the temperature, one can find out that different materials have various efficiencies. For the low-power case (Figure 3.4.a), the temperature reduction varies for different materials and the most reduction occurs by implementing SiO_2-TiO_2 DBR. The temperature increment for this structure is just 1K which is considerably low in comparison to the case of Tungsten without a DBR on top of it which is a 68K temperature rise. The counterpart results for the medium and high powers are shown in Figures 3.4.a and 3.4.b For these two cases, SiO_2-TiO_2 DBRs are the most efficient designs due to minimizing the maximum temperature. In the medium-power model, if Tungsten is exposed to light without a coating, its temperature increases from room temperature up to 467K. However, if the SiO_2-TiO_2 DBR is attached on top of that the temperature will rise to 300K and this represents for 167K temperature decline (Figure 3.4.b). By increasing the power, the temperature decreases more significantly compared to the case of Tungsten without coating exposed to the same light. For instance, in high- the power model (Figure 3.4.c), the maximum temperature reaches 1900 for the Tungsten, but for the optimized structure it drops to 720K which accounts for an 1180K decline in the maximum temperature.

(a)

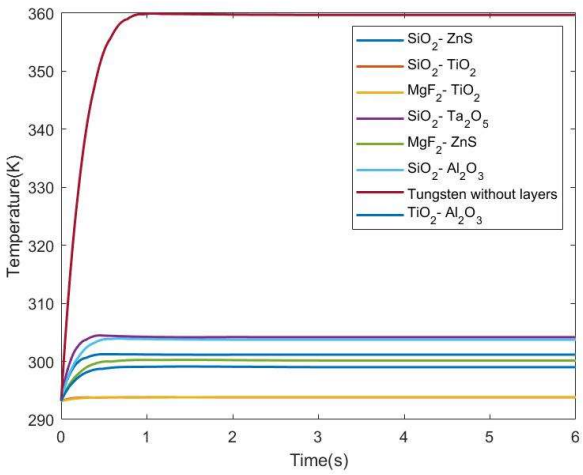

(b)

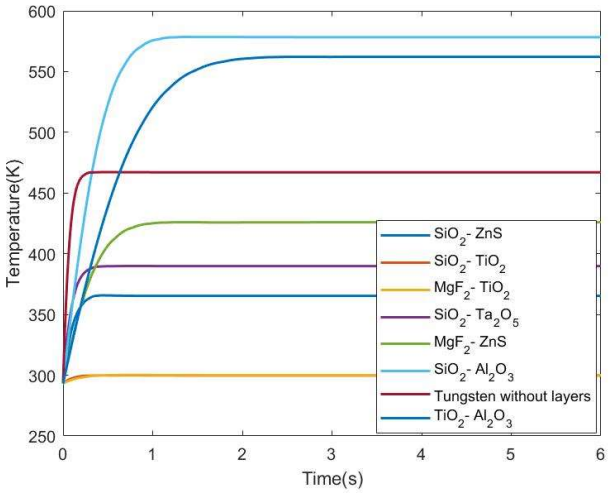

(c)

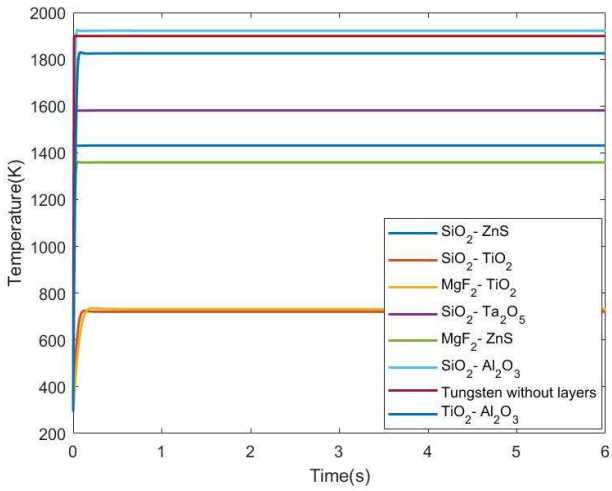

Figure 3.4. Temperature variation during the time for different material choices and a) Low-power, b) Medium-power, and c) High-power case.

An unexpected result is the temperature curves of the structure with Al_2O_3- SiO_2 periodic layers. Contrary to expectation, if we add these layers on top of the substrate the temperature of the structure will be increased instead of decreased in comparison to the structure without any coating. There are two explanations for this phenomenon. First, by increasing the temperature, the conductivity decreases in materials usually. Nevertheless, in ionic compounds, such as Al_2O_3, when temperature increases (over 400 K) the ions of the material become activated. These ions are charge carriers and with an increase in temperature, ionization increases, and hence, conductivity increase[112, 113]. Second, the reflectance of Al_2O_3- SiO_2 is high around 700 nm wavelength, where the laser operates. On the other hand, the broadband emissivity is lower compared to the other samples, as a result, it reduces the radiation heat transfer from the top surface. Therefore, the heat cannot leave the sample as easily as other samples and the temperature rises even more than the sample of Tungsten without a coating.

The incident angle is another important factor in studying the light reflected from a surface. Figure 3.5 illustrates the temperature change for different angles of incidents varying from 0 to 40 degrees. The proposed structure in this study is designed for 0 degrees. By decreasing the angle of the incident, the temperature decrement efficiency of the design improves. Based on the results, the best angle of the incident to achieve maximum reflection is 0 degrees.

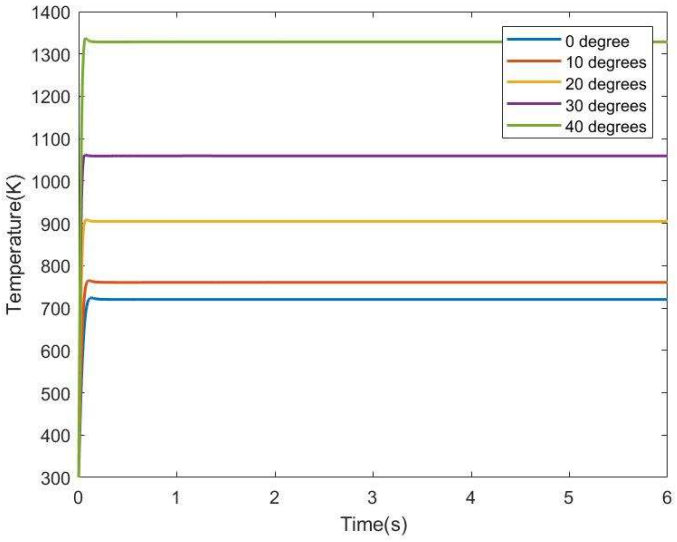

Figure 3.5. The comparison of the effect of the angle of incidence on the Temperature

In summary, as we concluded in chapter 2, it is undeniable that 10 layers of SiO_2- TiO_2 attached on top of the Tungsten decreases the temperature of the structure significantly and it is factual for different incident light powers and the different number of layers. However, by increasing the number of layers temperatures decreases progressively, and we need to consider other factors such as costs and efficiency which leads to picking 10 layers as the optimum number for our case. As an alternative choice, 10 layers of MgF_2/TiO_2 have roughly the same efficiency and can be employed. Moreover, using Al_2O_3- SiO_2 increases the temperature instead of decreasing it because of its ionic structure and low emissivity. Also, by decreasing the angle of the incident the temperature decrement efficiency of the design improves. Based on the results, the best angle of the incident to achieve maximum reflection is 0 degrees.

In this study, we prioritized the number of layers as a primary factor in the design of optical thin film filters, recognizing their direct impact on reflectivity. By emphasizing the significance of layer count, our aim was to underscore its crucial role in determining the overall performance of the filters. In order to establish the reliability of this approach, we conducted an investigation into the maximum temperature within the structure, considering various material pairs and different numbers of layers, in the high-power case. The findings are presented in Figure 3.6 to validate the notion that the emphasis on layer count and material choice does not compromise the overall results, ultimately highlighting that a configuration of 10 layers of SiO_2-TiO_2 emerges as the optimal solution.

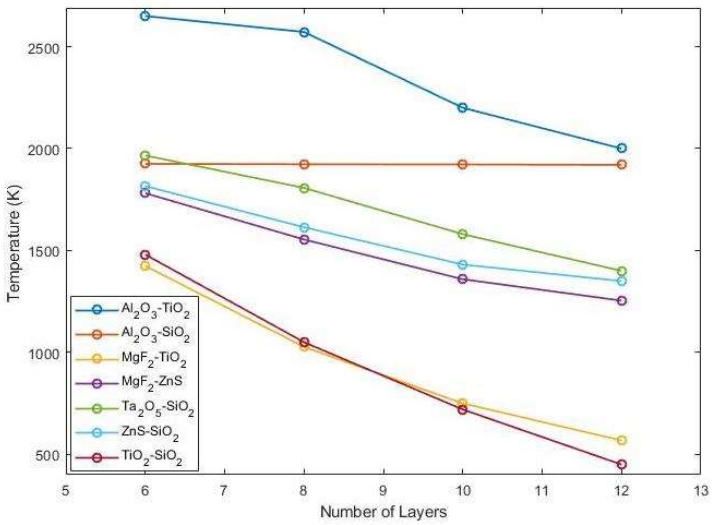

Figure 3.6. Temperature changes versus the number of layers for different pairs of materials.

4. AN OPTICAL STUDY ON ENHANCING REFLECTANCE OF REFRACTORY METALS BY PATTERNING

Distributed Bragg Reflectors (DBRs), as mentioned in previous chapters, have emerged as efficient components to manipulate and reflect light in different applications such as optical filters, offering exceptional reflectivity and precise control over light wavelengths. In chapter 2, a DBR has been designed to manage the temperature rise in the Tungsten substrate subjected to a high-power laser illumination. However, in the case of high-temperature operation of some optical applications such as high-power laser illuminations, the impact of thermal stresses on DBR performance arises as a challenge[67, 68]. These thermal stresses may lead the structure to expand which will cause peeling, deformation or other damages if there is no space for expansion[71]. This challenge can be addressed by patterning the DBR structure. Patterning allows to make some intervals in the structure so the expansion can happen freely and decrease the thermal stresses. Understanding and mitigating these thermal stresses are essential to achieve the full potential of DBRs in high-temperature applications.

On the other hand the, in the literature, various methods have been introduced to control the absorption and emission of the surface such as Multilayer thin-films[114], photonic crystals[115], metamaterials[116], nanotextured structures[117], surface roughening[31], and nanoparticles[118]. The patterning of the surface is one of the methods in various of studies to manipulate the absorption of the surface instead of using thin film coatings[119, 120]. However, there is a gap in studying the effect of implementation of patterns on the reflectance of the structure.

In this chapter, first, we will study the effect of the cavity layer on the performance of the DBR. Then we will combine this idea with the idea of the patterning the DBR.

4.1 Cavity enhanced DBR

A spacer or cavity layer is an intermediate layer with a specific thickness and refractive index that is intentionally designed to enhance the performance of the DBR[41]. It is typically inserted between different segments of DBRs to improve the optical performance of the whole structure[121]. This method may increase the reflectivity at the targeted wavelength or widen the reflectivity bandwidth. For instance, AlGaN/airgap DBRs have exhibited high reflectivity properties. Despite the numerous innovative approaches and successful outcomes in achieving broad-band and high-reflectance DBRs, the utilization of airgap DBRs has been primarily limited to studying the physics of cavities and their optical properties[122]. As an application for DBRs with air cavity, spectral filters and effectively filtering LED sources at specific wavelengths can be mentioned. Researchers analyzed resonances in cavities between two distributed Bragg reflectors (DBRs) using both theoretical and experimental methods. They modeled the reflectance and transmittance spectra of the cavity when represented by a one-dimensional photonic crystal made up of six bilayers of TiO_2/SiO_2 as a function of the cavity's thickness and refractive index. The reflectance spectra showed a broadband of high reflectance[123]. A schematic of this configuration has been shown in Figure 4.1.

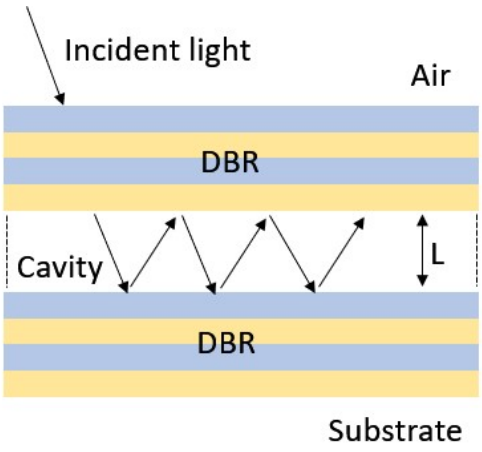

Figure 4.1. Multiple light beam reflections inside a cavity between two stacks of DBRs.

Fabry-Perot (FP) cavity consists of two parallel mirrors (such as DBRs) which is used for filtering specific wavelengths or as a resonator structure[124]. It is necessary to predict

resonant wavelengths in a Fabry-Perot structure. If the structure is one-dimensional, we use the Transfer Matrix Method (TMM). For higher dimensions, Finite-Difference Time-Domain (FDTD) or Finite Element Method (FEM) should be applied to determine peaks in the reflectivity plot[125]. In a FP cavity system, a dip in the reflection plots emerges due to the cavity resonance. The cavity modes are spaced at constant intervals in wavelength. As the angle of incident increases the wavelength of the FP modes changes.

Here we are interested in the effect of the cavity (spacer) layer between 10 layers of SiO_2/ TiO_2 DBR and the 1-micrometer Tungsten substrate. The spacer is assumed to be made of air. The only parameter that is important to be studied is the thickness of the cavity. A schematic of this configuration has been shown in Figure 4.2.

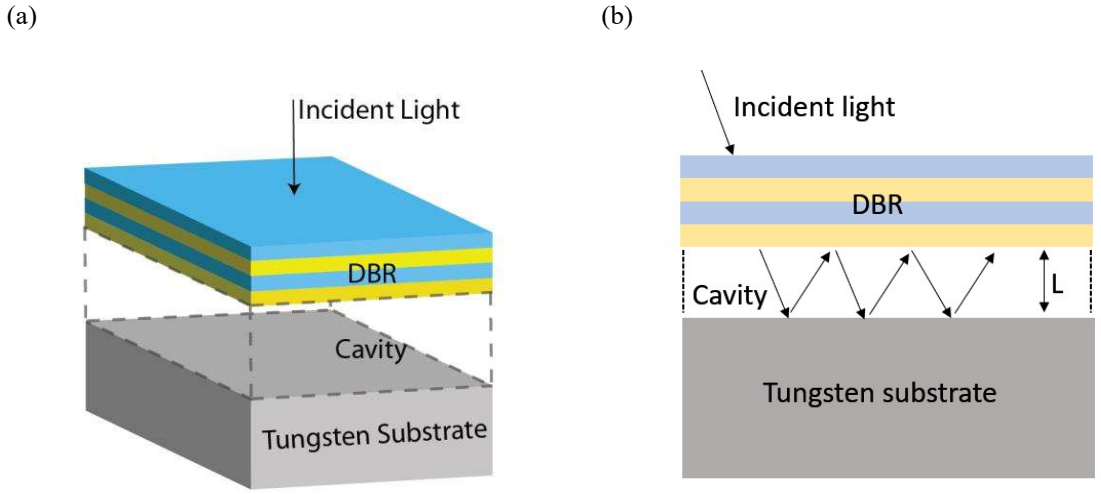

Figure 4.2. Schematic of unit cell of a cavity enhanced DBR on top of the Tungsten substrate. a) Oblique view, and b) Multiple reflections inside the cavity layer with the thickness of L.

Figure 4.3 shows the comparison of the reflectance for 4 different thicknesses and compares it with the one without a cavity layer. As one can see, by introducing a spacer layer the amplitude and bandwidth of the high-reflectance region have been widened almost in all cases. However, the best results are achieved when the thickness is 700 nm. This means that if the thickness is the same as the wavelength of the incident light. Also,

the result is promising when the thickness is 300 nm which is roughly half of the wavelength (350 nm).

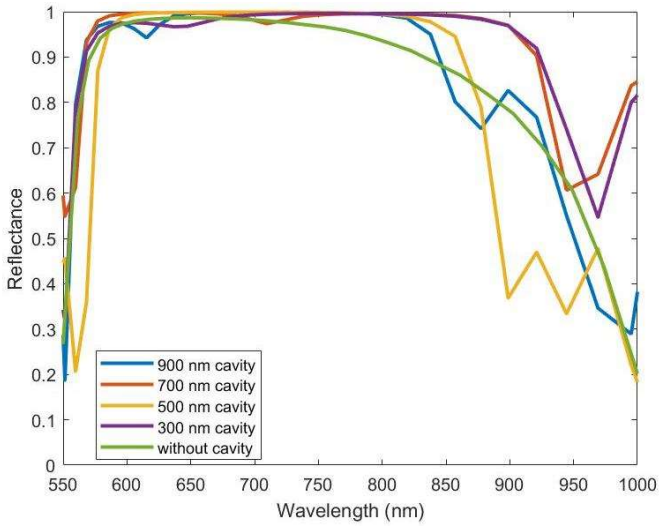

Figure 4.3. Reflectance comparison for different thicknesses of the cavity layer

Several optical phenomena occur inside the spacer that increases the reflectivity and its bandwidth. First, If the thickness of the spacer is chosen carefully a phase shift is possible to happen, which can affect the interferences within the structure. Second, the spacer layer affects the optical path length which is also effective in the interference phenomena. When a light beam enters the cavity, it travels backward and forward between two mirrors and makes several reflections. The interference of the reflected waves can be instructive or constructive which is dependent on the thickness of the spacer. Therefore, the implementation of a spacer layer can enhance reflectivity if it is designed carefully. DBR works with the same principle but the difference when adding a cavity layer to the DBR structure lies in the fine-tuning and optimization of the interference effects. The cavity layer introduces more control over the phase shift and optical path length within the resonant cavity. By adjusting the thickness of the cavity layer, the interference patterns can be precisely manipulated, leading to further enhancement of the constructive interference and increased reflectivity at specific wavelengths.

For a better understanding of the cavity enhanced reflection, it is advantageous to examine the propagation of electric fields within the structure, particularly focusing on the cavity layer. As shown in Figure 4.4, by increasing the cavity layer thickness from 300 nm to

700nm, the magnitude of electric field increases significantly from 2×10^4 to 7×10^4 V/m inside the cavity layer.

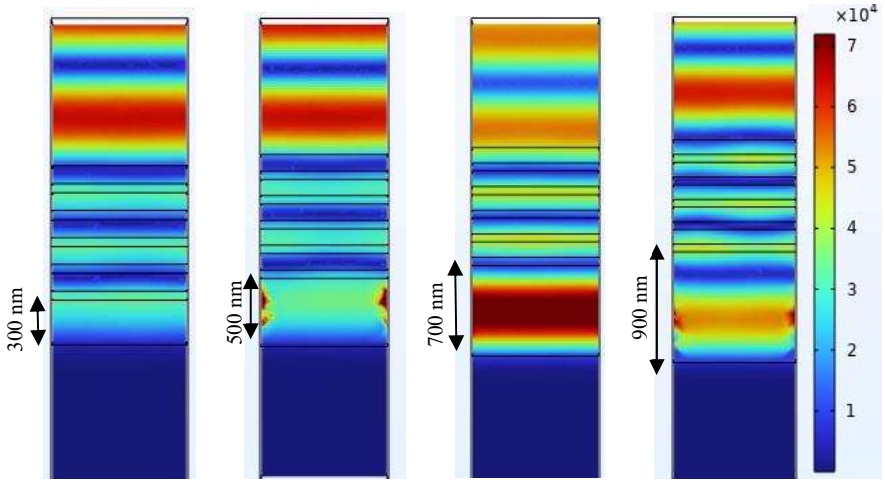

Figure 4.4. Electric field comparison for different thicknesses of the cavity layer

The condition for constructive interference after one round trip extorts a condition on the wavevector (k) perpendicular to the mirror surface. Because at higher angles there will be a wave vector parallel to the mirror surface, so the total wave number is larger than $\frac{2\pi}{\lambda}$ so the cavity frequencies increase. If the separation of the mirrors is L, then:

$$k.2L = 2m\pi \tag{4.1}$$

Hence[126]:

$$\omega = \frac{m\pi c}{L\sqrt{n_{cav}^2 - Sin^2\theta}} \tag{4.2}$$

Where n_{cav} is the refractive index of the cavity (air) which is 1 and m is an integer representing the modal order. Therefore:

$$L = \frac{m\lambda}{2\sqrt{n_{cav}^2 - Sin^2\theta}} \tag{4.3}$$

as the incident angle is 0, therefore the cavity length is:

$$L = \frac{m\lambda}{2} \tag{4.4}$$

In other words, a longitudinal resonant mode is a stationary electromagnetic wave if it can propagate in the cavity and has an integer number of halfwaves that fits into to the cavity (Figure 4.5). This confirms our simulation results that show thicknesses of 350 and 700 nm are best choices for our design.

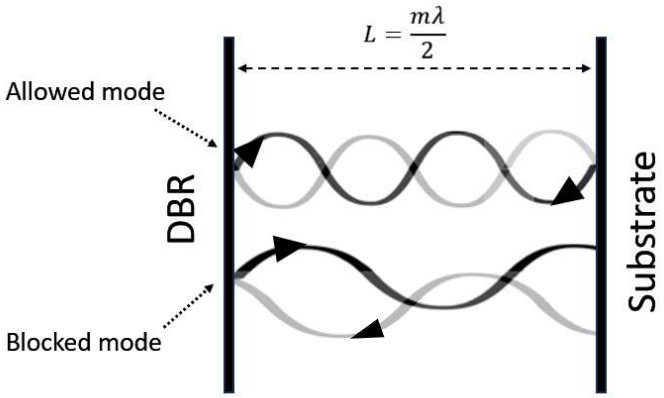

Figure 4.5. Allowed longitudinal resonant mode inside a cavity.

4.2 Patterned cavity enhanced DBR

One challenge that we face for the aforementioned model at higher temperature applications is the thermal stresses that causes expansions in the DBR layers[72]. Cracking due to a large mismatch of the thermal expansion between layers of the DBR and the substrate is the common failure mode[73, 74]. Also, one of the persistent problems that has been observed is the fragility of DBR layers, especially when exposed to thermal stresses. In this case, bubbling and cracking has been observed[76, 77]. On top of that, temperature increases may alter the reflection of the design by changing the refractive index of the layers under thermal stresses[78]. To overcome these issues, we can pattern the structure and make some empty areas in the design, so the layers are free to expand slightly without peeling or other defects. For example, while a coated substrate heats up or cools down, the stresses can be induced because of the difference in the thermal expansion coefficient between the layers which is controllable by patterning the

layers[80]. In the literature, considerable stress relief has been obtained by patterning the coating into rectangles and stripes[81]. With rectangular patterns the biaxial stress is degraded to a uniaxial stress and shape and size of the pattern is a key factor in stress reduction[82, 83]. A schematic of the periodic patterned design has been shown in Figure 4.6.

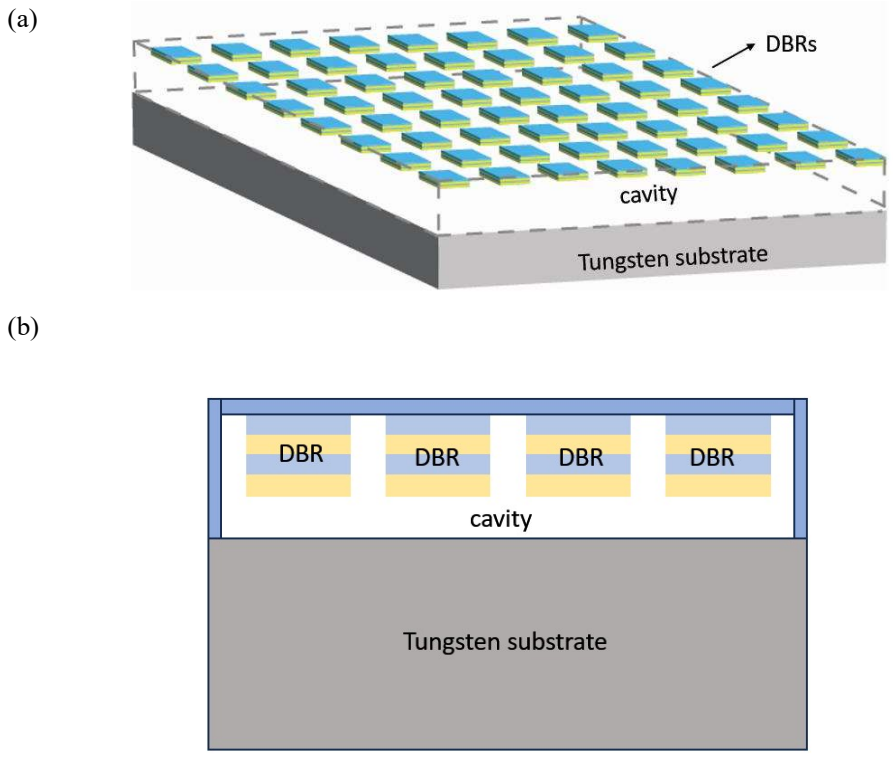

Figure 4.6. The periodic configuration of patterned cavity enhanced DBR configuration. A) An oblique view, and b) 2D view.

Here, we have a 1-micrometer cell of tungsten substrate that is under a 10-layer DBR and a cavity layer as before but the length and widths of DBR layers are 600×600 nm (Figure 4.7).

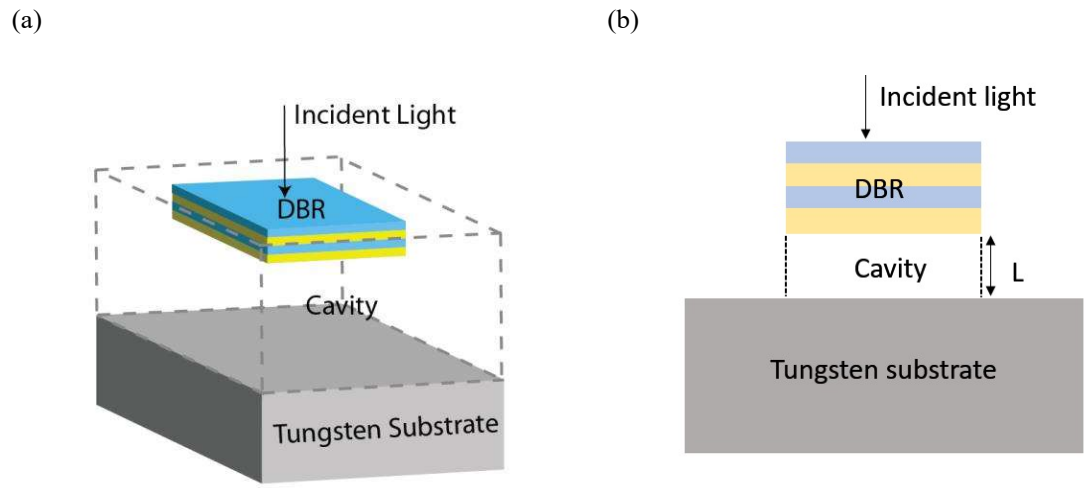

Figure 4.7. Schematic of unit cell of a cavity enhanced patterned DBR on top of the Tungsten substrate. a) Oblique view, and b) 2D view showing the cavity layer with the thickness of L.

Four different cases with different cavity thicknesses are studied and compared with the reflectance of the structure without cavity. As is shown in Figure 4.8, by introducing a cavity layer the overall reflectance increases. However, similar to Figure 4.3 the 700 nm cavity improves the reflection more than other cases. There is a peak in reflectance around 700 nm as a result of using the DBR that is enhanced by adding a 700 nm cavity layer from 0.45 to 0.75. This confirms the effectiveness of the cavity layer. Also, at higher wavelengths there is a dip around 1100 nm that is decreased significantly. Overall, broadband high-reflectance regions have been appeared for wavelengths between 600-1500 nm. It is worth mentioning that in the previous sections a reflectance of 90% was assumed as high quantity, however, in the current design 70% reflectance is accepted as high reflectance because the DBR is patterned, and its performance significantly decreases as its surface area decreases by patterning.

For a better understanding of the cavity enhanced reflection, it is advantageous to examine the propagation of electric fields within the structure. As shown in Figure4.9, by increasing the cavity layer thickness from 300 nm to 700nm, the magnitude of electric field inside the cavity and on the very top layer increases significantly due to the cavity resonance that happens at L=700nm. This increases the reflection of the structure. By increasing the cavity thickness from 700 to 900 nm the magnitude of the electric field decreases.

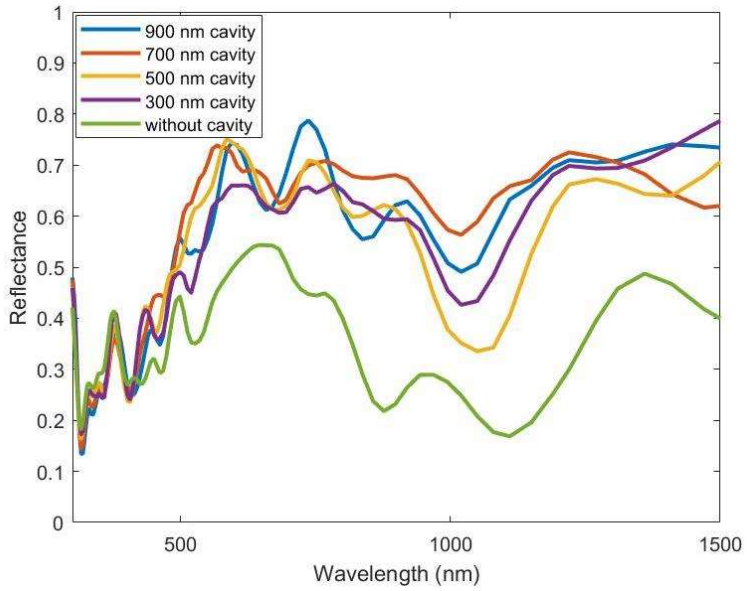

Figure 4.8. Reflectance comparison for different thicknesses of the cavity layer in patterned DBR structure.

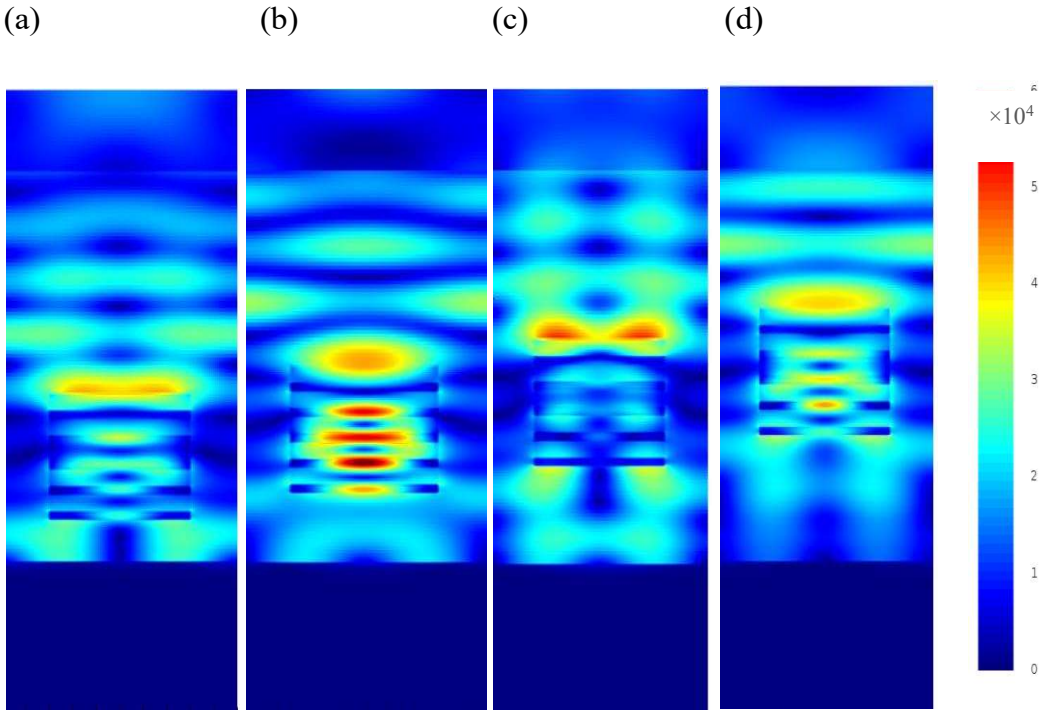

Figure 4.9. Electric field comparison for different thicknesses of the cavity layer a)300nm, b)500nm, c)700nm, and d)900nm.

In conclusion, the reflectivity of the refractory metal has been increased by enhancing the performance of the DBR. It has been done by using the advantage of implementing a cavity layer between the DBR and the refractory metal which was exposed to the incident light. This enhancement has been studied by varying thickness of the cavity layer. The highest efficiency is achieved when the cavity length is set to integer multiplications of half wavelength of the incident laser beam. As a result, the high reflection region has been widened from 580 up to 920 nm spectrum. Also, to prevent any damage caused by thermal stresses, the proposed structure has been patterned. By the aim of patterning there is free space between the unit cells of DBR so they can expand freely. Regarding the mentioned design the reflectance of the whole structure has been increased from 0.7 to 0.9.

5. CONCLUSION

In conclusion, in chapter 2, the reflectivity from the surface of Tungsten has been enhanced by the implementing of a DBR on the top surface of it which was exposed to the incident light. This enhancement is affected by several factors such as thickness, number, and material choice of the layers. The highest efficiency is achieved by using 10 layers of alternating high-index and low-index SiO_2/ TiO_2 thin films with thicknesses of 120 and 62 nm respectively. The reflectance of the structure has been increased from 0.46 to 0.96 (108% improvement). Also, the proposed structure in this study is designed for 0 degrees, and by increasing the incident angle 3 dips arise one of them is around our target wavelength. We concluded that the best angle of the incident to achieve maximum reflection is 0 degrees.

In chapter 3, we demonstrated that using 10 layers of SiO_2- TiO_2 on top of the Tungsten substrate decreases the temperature of the structure significantly and it is valid for different incident light powers and the different number of layers. As we increased the number of layers, maximum temperatures decreased. Nevertheless, we need to consider costs and efficiency and those make us pick 10 layers of the coatings as the optimum number for this research. Also, 10 layers of MgF_2/TiO_2 have remarkable efficiency and can be employed. Moreover, using Al_2O_3- SiO_2 increases the temperature instead of decreasing it because of its ionic structure and low emissivity. Again, another factor to be studied is the angle of incident light. By decreasing the angle of the incident, the temperature decreases more, as we expected. Based on the results, the best angle of the incident to achieve maximum reflection is 0 degrees.

In this study, we prioritized the number of layers as a primary factor in the design of optical thin film filters, because of its significant impact on reflectivity and to emphasize its role in determining the overall performance of the filters. To establish the reliability of this approach, we investigated the maximum temperature within the structure using different material pairs and numbers of layers, in the high-power case. The findings show that the emphasis on layer count and material choice does not

compromise the overall results, ultimately proving that a configuration of 10 layers of SiO_2-TiO_2 emerges as the optimal solution.

And finally, in chapter 4, a novel method for increasing the DBR performance has been introduced. the bandwidth of the reflectivity has been increased by the advantage of implementing a cavity layer between the DBR and the refractory metal which was exposed to the incident light. This enhancement has been studied by varying thickness of the cavity layer. The highest efficiency is achieved when the cavity length is set to integer multiplications of half wavelength of the incident laser beam and lead to constructive mode of the reflected beams. As a result, the high reflection region has been widened from 580 up to 920 nm spectrum. Also, to prevent any peeling caused by thermal stresses under high power laser illumination, the proposed structure has been patterned. The purpose of patterning is to make free spaces between the unit cells of DBR for expansion. Regarding the mentioned design the reflectance of the whole structure has been increased from 0.7 to 0.9.

Suggestions for future works

1. The adhesion of these coatings can present challenges, particularly under elevated temperatures due to the presence of thermal stresses. This indicates that the heat transferred between the layers is less than the other materials, so the thermal stresses are reduced significantly. On the other hand, if the coefficient of thermal expansion of two adjacent layers are similar it can promote better thermal adhesion. Achieving optimal thermal adhesion in a multilayer structure involves considering not only the coefficient of thermal expansion compatibility between the layers but also other factors that can impact adhesion. These factors include surface preparation, deposition techniques, interfacial bonding mechanisms, and the use of appropriate bonding materials or techniques. Within the scope of this study, we have not delved into the specific investigation of these aspects. Fabrication and testing of the designed configuration can be considered as future work.

2. The idea of increasing reflectivity by patterning which is explained in chapter 4 is a novel method that can be investigated more. Topology optimization methods can

be developed to enhance the performance of the structure. Fabrication criteria and concerns should be considered for further studies.

3. The idea of implementing a spacer layer between DBR and refractory metal can be investigated for different refractory metals and different types of reflectors rather than DBRs.

BIBLIOGRAPHY

1. Schmidt, F.F., *The engineering properties of tungsten and tungsten alloys*. Vol. 191. 1963: Defense Metals Information Center, Battelle Memorial Institute.
2. BROWN, T. and P. PITFIELD, *16. Tungsten.* Critical Metals Handbook, 1988: p. 385.
3. Saha, R. and W.D. Nix, *Effects of the substrate on the determination of thin film mechanical properties by nanoindentation.* Acta materialia, 2002. **50**(1): p. 23-38.
4. Raffo, P.L., *Yielding and fracture in tungsten and tungsten-rhenium alloys.* Journal of the Less Common Metals, 1969. **17**(2): p. 133-149.
5. El-Atwani, O., et al., *Outstanding radiation resistance of tungsten-based high-entropy alloys.* Science advances, 2019. **5**(3): p. eaav2002.
6. Kiran, U.R., et al., *Refractory metal alloying: A new method for improving mechanical properties of tungsten heavy alloys.* Journal of Alloys and Compounds, 2017. **709**: p. 609-619.
7. Lassner, E. and W.-D. Schubert, *Tungsten: properties, chemistry, technology of the elements, alloys, and chemical compounds*. 1999: Springer Science & Business Media.
8. Li, K.-c. and C. Wang, *Tungsten: its history, geology, ore-dressing, metallurgy, chemistry, analysis, applications, and economics*. 1955: Reinhold.
9. Sauvet, K., L. Sauques, and A. Rougier, *IR electrochromic WO3 thin films: from optimization to devices.* Solar Energy Materials and Solar Cells, 2009. **93**(12): p. 2045-2049.
10. Granqvist, C.G., *Handbook of inorganic electrochromic materials*. 1995: Elsevier.
11. Choo, R., J. Szekely, and R. Westhoff, *On the calculation of the free surface temperature of gas-tungsten-arc weld pools from first principles: Part I. Modeling the welding arc.* Metallurgical and Materials Transactions B, 1992. **23**(3): p. 357-369.
12. Ahmed, S.A., M. Mohsin, and S.M.Z. Ali, *Survey and technological analysis of laser and its defense applications.* Defence Technology, 2021. **17**(2): p. 583-592.
13. Davies, H., *The reflection of electromagnetic waves from a rough surface.* Proceedings of the IEE-Part IV: Institution Monographs, 1954. **101**(7): p. 209-214.
14. Keçebaş, M.A. and K. Şendur, *Enhancing the spectral reflectance of refractory metals by multilayer optical thin-film coatings.* JOSA B, 2018. **35**(8): p. 1845-1853.
15. Hsu, S.-C., et al., *Highly stable and efficient hybrid quantum dot light-emitting diodes.* IEEE Photonics Journal, 2015. **7**(5): p. 1-10.
16. Yan, C., et al., *Research on laser illumination based on phosphor in metal (PiM) by utilizing the boron nitride-coated copper foams.* ACS Applied Materials & Interfaces, 2021. **13**(25): p. 29996-30007.
17. Li, J., et al., *Photothermal Optimization of Quantum Dot Converters for High-Power Solid-State Light Sources.* Advanced Optical Materials, 2022. **10**(8): p. 2102201.
18. McDanels, D.L., *Tungsten fiber reinforced copper matrix composites: a review.* 1989.
19. Li, J.-S., et al., *Toward 200 lumens per watt of quantum-dot white-light-emitting diodes by reducing reabsorption loss.* ACS nano, 2020. **15**(1): p. 550-562.
20. Sahara, H., et al. *Opposed-cavity solar thermal thruster made of single crystal tungsten*. in *2001 International Electric Propulsion Conference, 27th IEPC, Pasadena, CA, USA, IEPC-01-214*. 2001.
21. Webb, J., *Thermal Analysis of a Tungsten Radiation Shield for Beamed Core*

Antimatter Rocketry. Embry Riddle Aeronautical University, 2002.
22. Rodrigues, J., et al., *Nitride and carbide of molybdenum and tungsten as substitutes of iridium for the catalysts used for space communication.* Catalysis letters, 1997. **45**(1-2): p. 1-3.
23. Klamm, B., *Passive space radiation shielding: Mass and volume optimization of tungsten-doped polyphenolic and polyethylene resins.* 2015.
24. Kotaki, Y. and H. Ishikawa, *Wavelength tunable DFB and DBR lasers for coherent optical fibre communications.* IEE Proceedings J: Optoelectronics, 1991. **138**(2): p. 171-177.
25. Ghosh, S., et al., *Design and modeling of high-performance DBR-based resonant-cavity-enhanced GeSn photodetector for fiber-optic telecommunication networks.* IEEE Sensors Journal, 2021. **21**(8): p. 9900-9908.
26. Costa, M.S., et al., *Effect of the Materials' Properties in the Design of High Transmittance and Low FWHM SiO2/TiO2 Thin Film Optical Filters for Integration in a Malaria Diagnostics Device.* BIODEVICES, 2021. **1**: p. 21-31.
27. Kitui, M., et al., *Optical Properties of TiO2 Based Multilayer Thin Films: Application to Optical Filters.* International Journal of Thin Film Science and Technology, 2015. **4**(1): p. 1.
28. Bousquet, P., F. Flory, and P. Roche, *Scattering from multilayer thin films: theory and experiment.* JOSA, 1981. **71**(9): p. 1115-1123.
29. Gao, X.-H., et al., *Microstructure and optical properties of SS/Mo/Al2O3 spectrally selective solar absorber coating.* Journal of Materials Engineering and Performance, 2017. **26**(1): p. 161-167.
30. Duparré, A. and S. Kassam, *Relation between light scattering and the microstructure of optical thin films.* Applied optics, 1993. **32**(28): p. 5475-5480.
31. Pirouzfam, N. and K. Sendur, *Tungsten Based Spectrally Selective Absorbers with Anisotropic Rough Surface Texture.* Nanomaterials, 2021. **11**(8): p. 2018.
32. Zaitsu, S.-i., et al., *Optical thin films consisting of nanoscale laminated layers.* Applied physics letters, 2002. **80**(14): p. 2442-2444.
33. Asghar, M., M. Khan, and S. Naseem, *Modeling thin film multilayer broad-band-pass filters in visible spectrum.* Czechoslovak journal of physics, 2003. **53**(12): p. 1209-1217.
34. Mwamburi, M., E. Wäckelgård, and B. Karlsson. *Optical properties of SnOx: F/Al2O3/Al solar selective reflector surfaces*. in *Third International ISES Europe Solar Congress, Copenhagen, Denmark*. 2000.
35. Mwamburi, M. and E. Wäckelgård, *Doped tin oxide coated aluminium solar selective reflector surfaces.* Solar Energy, 2000. **68**(4): p. 371-378.
36. Hosako, I., *Multilayer optical thin films for use at terahertz frequencies: method of fabrication.* Applied optics, 2005. **44**(18): p. 3769-3773.
37. Du, Y., et al., *Fabrication of 500 nm distributed Bragg reflector using Nb2O5-MgF2 multi-layer films.* Modern Physics Letters B, 2021. **35**(29): p. 2140001.
38. Ahmed, U., et al., *Investigation of spectral properties of dbr-based photonic crystal structure for optical filter application.* Crystals, 2022. **12**(3): p. 409.
39. Kunishi, W., et al., *Effect of the number of DBR layers on M 2 of photonic crystal lasers.* The Japan Society of Applied Physics, 2020.
40. Ahmed, N.M., M.R. Hashim, and H. Zainuriah. *Effects of layer thickness and incident angle variations on DBR reflectivity*. in *Materials science forum*. 2006. Trans Tech Publ.
41. Macleod, H.A. and H.A. Macleod, *Thin-film optical filters*. 2010: CRC press.
42. Asharchuk, I., et al., *Enchanced reflectance SiN $ _x $/SiO $ _x $ DBR mirror based on TEOS precursor fabricated by PECVD method.* arXiv preprint arXiv:2112.12525,

2021.
43. Xiao, L., et al., *WO3-Based Electrochromic Distributed Bragg Reflector: Toward Electrically Tunable Microcavity Luminescent Device.* Advanced Optical Materials, 2018. **6**(1): p. 1700791.
44. Al-Kuhaili, M., et al., *Transparent heat mirrors based on tungsten oxide–silver multilayer structures.* Solar energy, 2009. **83**(9): p. 1571-1577.
45. Pugliese, M., et al., *Highly Reflective Periodic Nanostructure Based on Thermal Evaporated Tungsten Oxide and Calcium Fluoride for Advanced Photonic Applications.* ACS Applied Nano Materials, 2020. **3**(11): p. 10978-10985.
46. Utsumi, Y., et al., *Tungsten–beryllium multilayer mirrors for soft x rays.* Applied optics, 1988. **27**(18): p. 3933-3936.
47. Gadhban, A.Q., H.M. Roomy, and S.K. Taha. *Design High performance multilayers cold mirror*. in *Journal of Physics: Conference Series*. 2021. IOP Publishing.
48. Shou, C., et al., *Investigation of a broadband TiO2/SiO2 optical thin-film filter for hybrid solar power systems.* Applied Energy, 2012. **92**: p. 298-306.
49. Lanfranchi, A., et al., *Multilayer Polymer Photonic Aegises Against Near-Infrared Solar Irradiation Heating.* ACS applied materials & interfaces, 2022. **14**(12): p. 14550-14560.
50. Kim, H., M. Kaya, and S. Hajimirza, *Broadband solar distributed Bragg reflector design using numerical optimization.* Solar Energy, 2021. **221**: p. 384-392.
51. Liang, H., et al., *Experimental investigation on spectral splitting of photovoltaic/thermal hybrid system with two-axis sun tracking based on SiO2/TiO2 interference thin film.* Energy Conversion and Management, 2019. **188**: p. 230-240.
52. Franssila, S., *Introduction to microfabrication*. 2010: John Wiley & Sons.
53. Clark, S.L. and P.T. Hammond, *Engineering the microfabrication of layer-by-layer thin films.* Advanced Materials, 1998. **10**(18): p. 1515-1519.
54. Gogova, D., *Optical and structural characterization of tungsten-based CVD metal oxide coatings.* Materials Letters, 1997. **30**(1): p. 109-113.
55. Hinczewski, D.S., et al., *Optical filters from SiO2 and TiO2 multi-layers using sol–gel spin coating method.* Solar energy materials and solar cells, 2005. **87**(1-4): p. 181-196.
56. Kumar, R. and A. Dixit, *All oxide sol-gel assisted SiO2/(ZnO/Sn-In2O3) n/SS dielectric/conducting multilayer based spectrally selective coating on Stainless Steel tubes for potential solar thermal application.* Solar Energy, 2022. **236**: p. 561-568.
57. Yepuri, V. and R. Dubey, *Transparent Dielectric TiO2/SiO2 Coatings for Thermal Shielding and Self-Cleaning Applications.* Kuwait Journal of Science, 2021.
58. Maghanga, C.M., et al., *Spectrally selective reflector surfaces for heat reduction in concentrator solar cells: modeling and applications of TiO 2: Nb-based thin films.* Applied optics, 2011. **50**(19): p. 3296-3302.
59. Kecebas, M.A., et al., *Passive radiative cooling design with broadband optical thin-film filters.* Journal of Quantitative Spectroscopy and Radiative Transfer, 2017. **198**: p. 179-186.
60. Böhnke, T., et al., *Surfaces with high solar reflectance and high thermal emittance on structured silicon for spacecraft thermal control.* Optical Materials, 2008. **30**(9): p. 1410-1421.
61. Zhang, L. and R.-m. Chen, *TiO2-Siloxane thermal control coatings for protection of spacecraft polymers.* Chinese Journal of Aeronautics, 2004. **17**(1): p. 53-59.
62. BenKahoul, M., et al. *Multilayer tuneable emittance coatings, with higher emittance for improved smart thermal control in space applications*. in *40th International Conference on Environmental Systems*. 2010.
63. Ryu, T.U., et al., *Optical, mechanical and thermal properties of MgF2-ZnS and*

MgF2-Ta2O5 composite thin films deposited by coevaporation. Optical Engineering, 2000. **39**(12): p. 3207-3213.
64. Butt, M.A., et al., *Modelling of multilayer dielectric filters based on TiO2/SiO2 and TiO2/MgF2 for fluorescence microscopy imaging.* Компьютерная оптика, 2016. **40**(5): p. 674-678.
65. Li, X., et al. *Preparation of MgF2, SiO2 and TiO2 Optical Films*. in *2022 2nd International Conference on Consumer Electronics and Computer Engineering (ICCECE)*. 2022. IEEE.
66. Koohestani, H., et al., *Synthesis and characterization of MgF2/Cu coating on aluminum produced by sputtering technique.* Mechanics of Advanced Composite Structures, 2022.
67. Chen, H., et al., *Laser plasma-induced damage characteristics of Ta 2 O 5 films.* Optical Materials Express, 2019. **9**(7): p. 3132-3145.
68. Ramesh, R., et al., *In Situ Temperature Dependent Optical Characterization and Modeling of Dealloyed Thin-Film Nanoporous Gold Absorbers.* Advanced Optical Materials, 2022. **10**(10): p. 2102479.
69. Minissale, M., et al., *The temperature dependence of optical properties of tungsten in the visible and near-infrared domains: an experimental and theoretical study.* Journal of Physics D: Applied Physics, 2017. **50**(45): p. 455601.
70. Dudley, J., D. Crawford, and J. Bowers, *Temperature dependence of the properties of DBR mirrors used in surface normal optoelectronic devices.* IEEE photonics technology letters, 1992. **4**(4): p. 311-314.
71. Zhou, Q., et al., *Material ejection and layer peeling-off in HfO2/SiO2 thin-film beam splitters induced by 1ω and 3ω lasers.* Optical Materials, 2022. **125**: p. 111894.
72. Nguyen, H.K., et al. *Reliability of high-power 1060-nm DBR lasers*. in *LEOS 2006-19th Annual Meeting of the IEEE Lasers and Electro-Optics Society*. 2006. IEEE.
73. Franke, A., et al. *Strain engineered high reflectivity DBRs in the deep UV*. in *Gallium Nitride Materials and Devices XI*. 2016. SPIE.
74. Huffaker, D., et al., *Sub-40 μA continuous-wave lasing in an oxidized vertical-cavity surface-emitting laser with dielectric mirrors.* IEEE Photonics Technology Letters, 1996. **8**(8): p. 974-976.
75. Nakada, N., et al., *Suppression of crack generation in GaN/AlGaN distributed Bragg reflector on sapphire by the insertion of GaN/AlGaN superlattice grown by metal-organic chemical vapor deposition.* Japanese journal of applied physics, 2003. **42**(2B): p. L144.
76. MacDougal, M.H. and P.D. Dapkus, *Wavelength shift of selectively oxidized Al/sub x/O/sub y/-AlGaAs-GaAs distributed Bragg reflectors.* IEEE Photonics Technology Letters, 1997. **9**(7): p. 884-886.
77. Markurt, T., et al., *A predictive model for plastic relaxation in (0001)-oriented wurtzite thin films and heterostructures.* Journal of Applied Physics, 2018. **124**(3).
78. Shen, J.L., et al., *Temperature dependence of the reflectivity in absorbing Bragg reflectors.* Optics express, 2001. **9**(6): p. 287-293.
79. Mosteiro, L., et al., *Density, speed of sound, refractive index and dielectric permittivity of (diethyl carbonate+ n-decane) at several temperatures.* The Journal of Chemical Thermodynamics, 2001. **33**(7): p. 787-801.
80. Yacobi, B., et al., *Stress relief in patterned GaAs grown on mismatched substrates.* Journal of Crystal Growth, 1989. **95**(1-4): p. 240-244.
81. De Boeck, J., et al., *Optical characterization of stress in narrow GaAs stripes on patterned Si substrates.* Applied physics letters, 1989. **55**(4): p. 365-367.
82. Van Der Ziel, J., N. Chand, and J. Weiner, *Reduction of Thermal Stress in Mbe Grown GaAs/Si by Patterning.* MRS Online Proceedings Library (OPL), 1989. **145**:

p. 317.
83. Van der Ziel, J., N. Chand, and J. Weiner, *Elimination of thermally induced biaxial stress in GaAs on Si layers by post-growth patterning.* Journal of applied physics, 1989. **66**(3): p. 1195-1198.
84. Nickel, A., D. Barnett, and F. Prinz, *Thermal stresses and deposition patterns in layered manufacturing.* Materials science and Engineering: A, 2001. **317**(1-2): p. 59-64.
85. Schade, P., H.M. Ortner, and I. Smid, *Refractory metals revolutionizing the lighting technology: A historical review.* International Journal of Refractory Metals and Hard Materials, 2015. **50**: p. 23-30.
86. Ataalla, M., et al., *Tungsten-based glasses for photochromic, electrochromic, gas sensors, and related applications: A review.* Journal of Non-Crystalline Solids, 2018. **491**: p. 43-54.
87. Zayats, A.V. and D. Richards, *Nano-optics and near-field optical microscopy*. 2009: Artech House.
88. Born, M. and E. Wolf, *Principles of optics: electromagnetic theory of propagation, interference and diffraction of light*. 2013: Elsevier.
89. Novotny, L. and B. Hecht, *Principles of nano-optics*. 2012: Cambridge university press.
90. Pierson, H.O., *Handbook of chemical vapor deposition: principles, technology and applications*. 1999: William Andrew.
91. Martin, P.M., *Handbook of deposition technologies for films and coatings: science, applications and technology*. 2009: William Andrew.
92. Bunshah, R.F. and C. Weissmantel, *Handbook of hard coatings*. Vol. 3. 2001: Noyes Publications Park Ridge, NJ.
93. COMSOL Multiphysics® v. 6. www.comsol.com. COMSOL AB, S., Sweden. Stockholm, Sweden
94. Melloni, A., et al., *The role of index contrast in dielectric optical waveguides.* International Journal of Materials and Product Technology, 2009. **34**(4): p. 421-437.
95. Dodge, M.J., *Refractive properties of magnesium fluoride.* Applied optics, 1984. **23**(12): p. 1980-1985.
96. Kumar, S., N. Verma, and M. Singla, *Reflective properties of ZnS nanoparticle coatings.* Journal of coatings technology and research, 2011. **8**(2): p. 223-228.
97. Salih, A.T., et al., *Single-material multilayer ZnS as anti-reflective coating for solar cell applications.* Optics Communications, 2017. **388**: p. 84-89.
98. Pai, Y.-H., C.-C. Chou, and F.-S. Shieu, *Preparation and optical properties of Ta2O5− x thin films.* Materials Chemistry and Physics, 2008. **107**(2-3): p. 524-527.
99. Chang, T.-H., et al., *Investigation of TiO2–Al2O3 bi-layer films as Bragg reflector of blue light by using electron beam evaporation.* Microsystem Technologies, 2018. **24**(10): p. 3941-3948.
100. Lan, Y., et al., *Fabrication of amorphous Al2O3 optical film with various refractive index and low surface roughness.* Materials Research Express, 2020. **7**(8): p. 086405.
101. Pimenta, S., et al., *Design and fabrication of SiO 2/TiO 2 and MgO/TiO 2 based high selective optical filters for diffuse reflectance and fluorescence signals extraction.* Biomedical optics express, 2015. **6**(8): p. 3084-3098.
102. Palik, E.D., *Handbook of optical constants of solids*. Vol. 3. 1998: Academic press.
103. Balanis, C.A., *Advanced engineering electromagnetics*. 2012: John Wiley & Sons.
104. Kennedy, M.W., et al. *Analytical and experimental validation of electromagnetic simulations using comsol®, re inductance, induction heating and magnetic fields*. in *COMSOL Users Conference, Stuttgart Germany*. 2011. Citeseer.

105. Xu, J., et al., *Design and Optimization of Red-light Reflector Using Simulation Software.* Sensors and Materials, 2021. **33**(8): p. 2619-2627.
106. Werner, W.S., K. Glantschnig, and C. Ambrosch-Draxl, *Optical constants and inelastic electron-scattering data for 17 elemental metals.* Journal of Physical and Chemical Reference Data, 2009. **38**(4): p. 1013-1092.
107. Assafli, H.T., A.H. Abdulhadi, and W.Y. Nassir, *Design High Efficient Reflectivity of Distributed Bragg Reflectors.* Iraqi J. Laser, 2016. **15**: p. 15-20.
108. Schubert, M.F., et al., *Distributed Bragg reflector consisting of high-and low-refractive-index thin film layers made of the same material.* Applied physics letters, 2007. **90**(14): p. 141115.
109. Kreith, F. and R.M. Manglik, *Principles of heat transfer*. 2016: Cengage learning.
110. Peng, Z., J.-Y. Hwang, and M. Andriese, *Magnetic loss in microwave heating.* Applied Physics Express, 2012. **5**(2): p. 027304.
111. Iliopoulos, A., et al. *Towards Selective Volumetric Additive Manufacturing and Processing of Ceramics*. in *International Design Engineering Technical Conferences and Computers and Information in Engineering Conference*. 2019. American Society of Mechanical Engineers.
112. Abu-Nada, E., *Effects of variable viscosity and thermal conductivity of Al2O3–water nanofluid on heat transfer enhancement in natural convection.* International Journal of Heat and Fluid Flow, 2009. **30**(4): p. 679-690.
113. Sulgani, M.T. and A. Karimipour, *Improve the thermal conductivity of 10w40-engine oil at various temperature by addition of Al2O3/Fe2O3 nanoparticles.* Journal of Molecular Liquids, 2019. **283**: p. 660-666.
114. Kecebas, M.A., et al., *Spectrally selective filter design for passive radiative cooling.* JOSA B, 2020. **37**(4): p. 1173-1182.
115. Celanovic, I., N. Jovanovic, and J. Kassakian, *Two-dimensional tungsten photonic crystals as selective thermal emitters.* Applied Physics Letters, 2008. **92**(19).
116. Wang, H., et al., *Highly efficient selective metamaterial absorber for high-temperature solar thermal energy harvesting.* Solar Energy Materials and Solar Cells, 2015. **137**: p. 235-242.
117. Gupta, M.C., et al., *Optical nanostructures design, fabrication, and applications for solar/thermal energy conversion.* Solar Energy, 2018. **165**: p. 100-114.
118. Shah, A.A. and M.C. Gupta, *Spectral selective surfaces for concentrated solar power receivers by laser sintering of tungsten micro and nano particles.* Solar energy materials and solar cells, 2013. **117**: p. 489-493.
119. Chen, M., et al., *Enhancing infrared emission behavior of polymer coatings for radiative cooling applications.* Journal of Physics D: Applied Physics, 2021. **54**(29): p. 295501.
120. Liu, Y., J. Li, and C. Liu, *Surface pattern over a thick silica film to realize passive radiative cooling.* Materials, 2021. **14**(10): p. 2637.
121. Ma, Y., et al., *Highly sensitive acetylene detection based on multi-pass retro-reflection-cavity-enhanced photoacoustic spectroscopy and a fiber amplified diode laser.* Optics Express, 2019. **27**(10): p. 14163-14172.
122. Zhang, C., R. ElAfandy, and J. Han, *Distributed Bragg reflectors for GaN-based vertical-cavity surface-emitting lasers.* Applied Sciences, 2019. **9**(8): p. 1593.
123. Gryga, M., D. Ciprian, and P. Hlubina, *Distributed Bragg reflectors employed in sensors and filters based on cavity-mode spectral-domain resonances.* Sensors, 2022. **22**(10): p. 3627.
124. Barrios, C.A., et al., *Compact silicon tunable Fabry-Perot resonator with low power consumption.* IEEE Photonics Technology Letters, 2004. **16**(2): p. 506-508.
125. Kim, J.H.E., et al., *DBR, Sub-wavelength grating, and Photonic crystal slab Fabry-*

Perot cavity design using phase analysis by FDTD. Optics express, 2007. **15**(16): p. 10330-10339.
126. Giordano, G., *design and characterization of organic electrocutions microcavitie*. 2016.